2022-11

Study of gamma ray signals from primordial black hole evaporation

Recabarren Vergara, Luis Matías

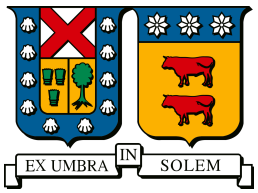

Universidad Técnica Federico Santa María

Departamento de Física

Study of gamma ray signals from primordial black hole evaporation

Thesis submitted to the Physics Department, Universidad Técnica Federico Santa María, for the degree of Master in Science majored in Physics

Author: Luis M. Recabarren
Committee: Claudio Dib (Advisor)
Alfonso Zerwekh
Andreas Reisenegger

November, 2022

Abstract

In this work, we study the photon spectrum produced by the Hawking radiation from a primordial black hole (PBH). We focus on the last stages before full evaporation. The spectrum is estimated using the black body approach and Hawking's emission formula. The connection between both descriptions is discussed. Furthermore, through analytical approximations for the greybody factors at the high and low energy limits, we time-integrate the primary spectrum along the PBH lifetime. As a result, we obtain a correction to the primary photon time-integrated spectrum commonly used in the literature. In addition, due to the BH emission of free quarks, we estimate, under rough approximations, the pion production from quark hadronization. As a consequence, a secondary photon spectrum is obtained through $\pi^0 \to \gamma\gamma$ decay. These calculations for the spectral emission are compared with spectra obtained with simulations using `BlackHawk`. Based on the previous analysis, we estimate the number of photons per km^2, within a certain detection energy interval, and during a fixed observation time, that eventually reach the Earth's atmosphere. Finally, with the help of `Corsika`, we run simulations of very high energy gamma rays to study the basic features of the electromagnetic showers that are produced in the atmosphere.

Contents

"An expert is a person who has found out by his own painful experience all the mistakes that one can make in a very narrow field."

N. Bohr

1 Introduction

1.1 Black Hole temperature

Black holes are solutions of Einstein's field equations for a point-like mass source in the theory of general relativity. These solutions describe a region of spacetime delimited by an event horizon, inside of which nothing can escape. The simplest solution is for the Schwarzschild metric, which applies to a nonrotating and uncharged object of mass M. The corresponding event horizon is:

$$r_s = \frac{2GM}{c^2}, \tag{1}$$

which is called Schwarzschild radius. Here, G is the gravitational constant and c the speed of light in vacuum. There are other solutions with angular momentum and electric charge. Today we know that these compact objects exist. Indeed, we can measure the effects they produce in their proximity. For example, measuring orbits of stars near the center of our galaxy, we can estimate the mass of the super massive BH located at that center, resulting in 4 million of solar masses. Although general relativity allows for BHs of any mass, stellar evolution leads to collapse into BHs only for objects heavier than a few solar masses. However, there is a scenario where BH masses can be arbitrarily small, even down to the Planck mass scale ($\sim 10^{-5}$ g). Such scenario would be at early stages of the Universe, where fluctuactions could cause mass overdensities in regions inside the Schwarzschild radius, resulting in a compact object called primordial black hole (PBH) [23] [6]. PBHs have gained interest in recent years because they are good candidates for partial or even total component of dark matter [7, 20].

Thermodynamics describes a system from a macroscopic approach using a few state variables. These quantities are averages of fundamental physics quantities. However, there is an underlying microscopic description, called statistical mechanics, which is based on quantum mechanics. For example, a cavity with a certain temperature radiates photons because the material of its walls contains electrons that can interact electromagnetically with photons. This is how quantum electrodynamics explains the black body radiation. Following this line of reasoning, the thermodynamics of black holes, with mass (M), angular momentum (J) and electric charge (Q) as state variables, should also have a quantum description. This is related to the problem of a quantum theory of gravity. A first try for this description is the work of S. Hawking in 1974 [12]. He applied quantum field theory in curved spaces, but holding the metric classical. Hawking found that an external observer should measure a radiation coming out from a BH[1].

[1]This phenomenon is similar to the bath of thermal radiation that an accelerated observer experiences falling into a black hole. This is called the Unruh effect.

Such radiation follows a Planckian spectrum with temperature given by

$$kT = \frac{\hbar c^3}{8\pi G M} = 1.06 \left(\frac{10^{10}\,\mathrm{kg}}{M} \right) \mathrm{GeV}, \tag{2}$$

where $\hbar$ is the reduced Planck constant and k is the Boltzmann constant. An intuitive way to understand the origin of this radiation comes from the particle-antiparticle pair creation. If the Compton wavelength of created particles is less than the BH radius (Equation (1)), particles with negative energy fall into the hole, whereas particles with positive energy escape to infinity. The reverse process is not allowed because energy conservation demands that real particles with negative energy must have a decreasing radial coordinate, a condition that is satisfied for particles inside the event horizon (see Ref. [18] for details). The BH temperature defined in Equation (2) encodes a deep physical meaning. First, it provides a consistent unification of gravity and thermodynamics. Consider a Schwarzschild black hole with an area

$$\begin{aligned} A &= 4\pi r_s^2 \\ &= \frac{16\pi G^2 M^2}{c^4}. \end{aligned} \tag{3}$$

Under a change in mass dM, the area changes accordingly:

$$dA = \frac{32\pi G^2 M}{c^4}\, dM. \tag{4}$$

In terms of BH temperature

$$\begin{aligned} dM &= \frac{ckT}{4\hbar G}\, dA \\ d(Mc^2) &= T\, d\left(\frac{Akc^3}{4\hbar G} \right). \end{aligned} \tag{5}$$

Using the first law of thermodynamics in the form $dE = T\, dS$, we obtain the entropy for black holes

$$S = \frac{kc^3}{4\hbar G}\, A. \tag{6}$$

Altough J. Beckenstein derived an approximate value of the BH entropy years earlier [4], Hawking obtained the 1/4 factor of the BH entropy formula.

According to the second law of thermodynamics, the entropy never decreases for a closed system. Therefore we should have

$$\frac{dA}{dt} \geq 0. \tag{7}$$

Second, Hawking's theory allows for the possibility that BHs can dissapear. The energy loss in radiation causes the decrease of its mass and consequently its downsizing. This process increases the temperature, accelerating this emission towards the end until full evaporation. One might think that Hawking radiation violates the second law of thermodynamics given the area downsizing ($A \propto r_s^2 \propto M^2$). This is not correct, because a radiating BH cannot be regarded as an isolated system. As we shall demonstrate later, the rate of mass loss given by this radiation mechanism is:

$$\frac{dM}{dt} = -\frac{\alpha}{M^2}, \tag{8}$$

where α is

$$\alpha = \frac{\hbar c^4}{15360\pi G^2} = 4 \times 10^{15}\ \mathrm{kg^3 s^{-1}}. \tag{9}$$

After integrating Equation (8), we obtain

$$M^3(t) - M_0^3 = -3\,\alpha\,(t - t_0) \qquad t > t_0. \tag{10}$$

Here, M_0 is the initial mass at time t_0 and $M(t)$ is the mass after a time interval $(t - t_0)$. If $M(t) = 0$, the BH has evaporated after lifetime $\tau \equiv t - t_0$. Therefore a relation between lifetime and respective initial mass is found:

$$\tau \approx \frac{M_0^3}{3\alpha} \approx\ 10^{-24} \left(\frac{M}{\mathrm{kg}}\right)^3\ \mathrm{yr}. \tag{11}$$

The time needed for a BH to decrease its mass by half is:

$$t_{M/2} = \frac{1}{3\alpha}\left(M_0^3 - \frac{M_0^3}{8}\right) = \frac{7}{8}\,\tau. \tag{12}$$

This result gives us an idea of how accelerated the phenomenon becomes in its last stages before full evaporation. For example, a BH of 1 solar mass $\sim 10^{30}$ kg has a lifetime of $\sim 10^{66}$ yr (much larger than the age of the Universe), and a temperature of about 10^{-7} K. As a consequence, all known BHs are colder than the Universe, so they absorb instead of emitting radiation. However, for PBHs with masses of the order of $M_0 \lesssim 2 \times 10^{11}$ kg, their lifetimes are comparable to the age of the Universe ($\tau \sim 10^{10}$ yr), and therefore they should have evaporated by now.

1.2 The black body approximation

As a first approximation, the rate of particle emission can be estimated treating the BH radiation like a boson/fermion gas. While black body radiation usually refers to thermal emittion of photons only, we emphasize that a BH radiates all Standard Model particles, with relative rates depending of BH temperature and particles masses. We shall call this approach the black body approximation. The states of a particle can be specified by its momentum and spin. The average number of particles of species i, per unit volume with momentum in the range $[\vec{p},\ \vec{p}+d\vec{p}]$, and g_i degrees of freedom (polarizations) is

$$dn_i = \frac{g_i}{h^3}\, d^3p\, f_p^{(i)}\,, \tag{13}$$

where $f_p^{(i)}$ is the occupation number (number of particles in a given state of momentum $\vec{p}$)

$$f_p^{(i)} = \frac{1}{e^{(E_p-\mu)/kT} \pm 1}, \tag{14}$$

where the sign $-$ $(+)$ holds for bosons (fermions). Here, T is the temperature and μ the chemical potential. For photons, $g_\gamma = 2$, $\mu = 0$ and $E_p = pc$. Then we write

$$\begin{aligned} n_\gamma &= \frac{2}{h^3} \int d\Omega_p \int_0^\infty dp\, \frac{p^2}{e^{\,pc/kT}-1} \\ &= \frac{8\pi}{h^3} \int_0^\infty dp\, \frac{p^2}{e^{\,pc/kT}-1}. \end{aligned} \tag{15}$$

Using $x = pc/kT$

$$\begin{aligned} n_\gamma &= 8\pi \left(\frac{kT}{2\pi\hbar c}\right)^3 \int_0^\infty dx\, \frac{x^2}{e^x-1} \\ &= \frac{2}{\pi^2}\left(\frac{kT}{\hbar c}\right)^3 \zeta(3), \end{aligned} \tag{16}$$

where in the last line we have used the identity

$$\int_0^\infty dx\, \frac{x^{n-1}}{e^x + a} = \begin{cases} \Gamma(n)\,\zeta(n) & a = -1 \\ \Gamma(n)\,\eta(n) & a = +1 \end{cases} \tag{17}$$

where $\zeta(n)$ is the Riemann zeta function, and η is the Dirichlet eta function. Both functions are related through

$$\eta(n) = (1 - 2^{1-n})\,\zeta(n). \tag{18}$$

Using the same procedure, assuming massless electrons, their number density is

$$n_e = \frac{3}{2\pi^2}\left(\frac{kT}{\hbar c}\right)^3 \zeta(3). \tag{19}$$

Now, let us consider the flux through an area A due to outgoing particles from a thermal cavity, of particles with momentum $\vec{p}$, in a time interval Δt as Figure 1 shows.

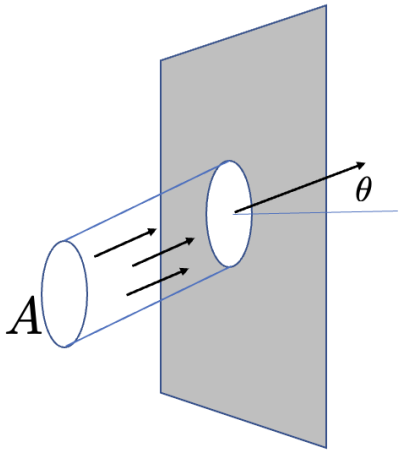

Figure 1: Emission of particles from a cavity through a hole of area A. The particles considered are inside a skewed cylinder of base A and height $c\cos\theta\,\Delta t$.

Of the particles with momentum $\vec{p}$ (that we have assumed massless), only those inside the cylinder of Figure 1, can cross a hole of area A in time Δt. This can be written as

$$dN_A = dn \times (A\; c\cos\theta\Delta t). \tag{20}$$

The spectral flux density j_i (number of particles with energy $E = pc$, in the range $[\,E,\; E{+}dE\,]$ that cross the section per unit area and time) is obtained by integrating the contributions of all momentum directions. Note that to cover all directions of outgoing particles, the

integration in θ is over one hemisphere only.

$$\begin{aligned} dj_i &= \int_{\text{all dir}} \frac{dN_A}{A\Delta t} \\ &= g_i \frac{c}{h^3} dp\ p^2 f_p^{(i)} \int_0^{2\pi} d\phi \int_0^1 d(\cos\theta) \cos\theta \\ &= g_i \frac{\pi c}{h^3} dp\ p^2 f_p^{(i)} \\ &= \frac{c}{4}\, dn_i. \end{aligned} \tag{21}$$

From the last line it is clear that the flux density is a factor $c/4$ of the average number of particles per unit volume. The spectral emission can be obtained by inserting the spectral form of dn_i (Equation (13)). Then we write

$$\begin{aligned} d\dot{N}_i &= A\, dj_i \\ &= A\, \frac{g_i c}{4h^3}\, d^3p\, f_p^{(i)}. \end{aligned} \tag{22}$$

Here, A corresponds to the BH event horizon area

$$A = \frac{16\pi G^2 M^2}{c^4} = \frac{\hbar^2 c^2}{4\pi k^2 T^2}. \tag{23}$$

Using

$$p^2 dp = \frac{p}{c^2} E dE \quad , \quad p = \sqrt{E^2 - (m_i c^2)^2}/c, \tag{24}$$

and inserting the area in Equation (22), the spectral emission rate is:

$$\begin{aligned} d\dot{N}_i &= \frac{g_i}{h}\, \Gamma(M,E) f_p^{(i)}\, dE \\ \Rightarrow \frac{d\dot{N}_i}{dE} &= \frac{g_i}{h}\, \frac{\Gamma(M,E)}{e^{\,E_p/kT} \pm 1}, \end{aligned} \tag{25}$$

where we have defined the absorption coefficient $\Gamma(M,E)$ as

$$\Gamma(M,E) = \frac{4G^2 M^2 pE}{\hbar^2 c^5} \quad , \quad p = \sqrt{E^2 - (m_i c^2)^2}/c. \tag{26}$$

We must remark that this expression for absorption coefficient is only aplicable to *large size* black body emitters (cavities much large than the usual wavelengths, i.e, the geometrical optics limit). For BHs, $\Gamma(M, E)$ function is different, as we will see below.

For massless particles ($p = E/c$) the absorption coefficient is

$$\Gamma(M, E) = \frac{4G^2M^2E^2}{\hbar^2c^6}. \tag{27}$$

Inserting in Equation (25), and setting $g_i = 2$ for photons, we obtain the spectral emission rate of a black body with temperature T_{BH} (in the approximation of geometrical optics limit)

$$\frac{d\dot{N}_\gamma}{dE} = \frac{4G^2M^2E^2}{\pi\hbar^3c^6}\frac{1}{e^{E_p/kT_{BH}} - 1}. \tag{28}$$

1.3 Hawking's emission formula

According Hawking's theory, the radiation coming from a BH can be understood by means of creation of particle-antiparticle pairs near the event horizon [13]. This is due to vacuum quantum fluctuations. Particles with negative energy can enter the horizon and fall into the hole, decreasing the BH energy as a result. Particles with positive energy escape to infinity being observed as radiation. Nevertheless, the intense gravitational field of a BH could absorb a large amount of them, reducing the spectral emission. Therefore, in comparison with a black body of temperature T_{BH}, the Hawking spectrum is less intense.

The spectral emission rate of particles of species i emitted by a BH of mass M, electric charge Q, and angular momentum J is:

$$\frac{d\dot{N}_i}{dE} = \frac{g_i}{h}\frac{\Gamma_{s_i}(M, E)}{e^x \pm 1} \quad , \quad x = \frac{E - J\Omega - Q\Phi}{kT}, \tag{29}$$

where s_i is the particle spin, Ω and Φ are the angular velocity and electric potential. The sign $-$ $(+)$ holds for bosons (fermions). The coefficient $\Gamma_{s_i}(M, E)$ measures the probability that a particle of species i and spin s, could escape to infinity instead of being absorbed by the BH. This absorption coefficient does not have an analytical expression. However, for massless particles emitted by nonrotating uncharged BHs, analytical approximations of the absorption coefficient at asymptotic values of energy can be found [16]. In the limit $E \ll kT$

it holds:

$$\Gamma_s(M,E)_{\,E\ll kT} = \begin{cases} \frac{16G^2M^2E^2}{\hbar^2c^6} & s=0 \\ \frac{2G^2M^2E^2}{\hbar^2c^6} & s=\frac{1}{2} \\ \frac{64G^4M^4E^4}{3\hbar^4c^{12}} & s=1 \\ \frac{256G^6M^6E^6}{45\hbar^6c^{18}} & s=2, \end{cases} \tag{30}$$

whereas in the limit $E \gg kT$ this factor approaches to:

$$\Gamma(M,E)_{\,E\gg kT} = \frac{27G^2M^2E^2}{\hbar^2c^6} \tag{31}$$

for all species. This limit is called the geometrical optics limit because $\lambda \ll r_s$. In this energy regime, the black body radiation should be recovered. Given that $\Gamma_s(M,E)$ deviates the BH spectrum from a thermal spectrum (black body), this coefficient is also called greybody factor. Notice that using both approximations for the greybody factor, the BH spectrum (Equation (29)) preserves the invariance with respect to the quantity E/kT. This feature leaves the maximum of the spectral emission rate equal for all BH temperature, as we will see in Section 4.

We are interested in Schwarzschild BHs, which are nonrotating and uncharged. Then, Hawking's formula for the spectral emission rate can be written as

$$\frac{d\dot{N}_i}{dE} = \frac{g_i}{h}\,\frac{\Gamma_{s_i}(M,E)}{e^{\,E/kT}\pm 1}. \tag{32}$$

If we focus on particles with energy $E \gg kT$, the $\Gamma_{s_i}(M,E)$ factor can be approximated by Equation (31). Thus

$$\frac{d\dot{N}_i}{dE} = \frac{g_i}{h}\,\frac{27G^2M^2}{\hbar^2c^6}\,\frac{E^2}{e^{\,E/kT}\pm 1} \quad \text{for} \quad E \gg kT. \tag{33}$$

In comparison with the black body approach (Equation (25)), for massless particles we find

$$\frac{d\dot{N}_i}{dE}^{\,(\mathrm{H})} = \frac{27}{4}\,\frac{d\dot{N}_i}{dE}^{\,(\mathrm{BB})} \quad \text{for} \quad E \gg kT, \tag{34}$$

where superscript (H) is for Hawking's approximation and (BB) for the black body approximation. This result is very interesting because the spectrum for photons with energies $E_\gamma \gg kT_{BH}$ is $27/4 \approx 7$ times more intense than a black body with temperature T_{BH}. This fact can be attributed to the coefficient $\Gamma_s(M, E)$. From Equations (27) and (31) it is satisfied:

$$\Gamma^{(H)} = \frac{27}{4}\Gamma^{(BB)} \quad \text{for} \quad E \gg kT. \tag{35}$$

This unexpected result raises questions about the correct values of greybody factors at the geometrical optics limit, where black body radiation is valid. This result may induce us to think that black holes would emit more than a black body of same temperature. However, as we shall see in Section 4, BHs emit less at lower energies.

1.4 Rate of mass loss

The mass-temperature relation can be used to obtain a dynamical Equation for the BH mass loss. Let us suppose that BH emits like a black body. Applying the Stefan-Boltzmann law, the total radiated power per unit surface (total energy flux) is

$$\mathcal{I} = \sigma T^4 = \frac{\sigma}{k^4}\left(\frac{\hbar c^3}{8\pi GM}\right)^4, \tag{36}$$

where σ is the Stefan-Boltzmann constant. Inserting its value and multiplying by the BH horizon area A (Equation (23)), we obtain the total power radiated

$$\begin{aligned} \mathcal{P} &= A\mathcal{I} \\ &= \frac{16\pi G^2 M^2}{c^4}\,\frac{\pi^2}{60\hbar^3 c^2}\left(\frac{\hbar c^3}{8\pi GM}\right)^4 \\ &= \frac{\hbar c^6}{15360\pi G^2}\,\frac{1}{M^2}. \end{aligned} \tag{37}$$

This expression is often found in literature. However, as stated above, it considers the $\Gamma(M, E)$ factor as a usual black body cavity, which is not applicable to BH radiation. Despite this caveat, let us continue the calculation for pedagogical reasons. Using energy conservation, the total power radiated $\mathcal{P}$ is equal to the rate of mass-energy loss according to

$$\mathcal{P} = -\frac{d}{dt}Mc^2. \tag{38}$$

In comparison with Equation (37) we obtain

$$\frac{dM}{dt} = -\frac{\alpha}{M^2} \tag{39}$$

with

$$\alpha = \frac{\hbar c^4}{15360\pi G^2} = 4 \times 10^{15}\ \frac{\mathrm{kg}^3}{\mathrm{s}}. \tag{40}$$

This expression for α would correspond to a BH emitting photons only, and with the assumption of a black body absorption coefficient. In the general case, α depends on the BH temperature and the masses of all kinds of emited particles. Let us find the contributtion to α for the emission of bosons and fermions. The energy density (the average energy per unit volume) of particle species i with momentum in the range $[\vec{p}, \vec{p} + d\vec{p}]$ can be defined as

$$\begin{aligned} du_i &= dn_i\, E_p \\ &= \frac{g_i}{h^3} d^3p\, f_p^{(i)}\, E_p, \end{aligned} \tag{41}$$

where dn_i is the spectral number density, Equation (13). Just as the flux density j_i is $c/4$ times the number density (Equation (21)), the irradiance $\mathcal{I}$ (energy per unit area and time) is

$$\begin{aligned} d\mathcal{I}_i &= \frac{c}{4}\, du_i \\ &= \frac{c}{4}\, \frac{g_i}{h^3} d^3p\, f_p^{(i)}\, E_p. \end{aligned} \tag{42}$$

The total power emitted by a BH is the sum over all species and integration over all momenta, multiplied by the BH horizon area A,

$$\mathcal{P} = A \sum_i \int d\mathcal{I}_i. \tag{43}$$

Inserting Equation (42) and the value of A (Equation (23)) we obtain

$$\mathcal{P} = \sum_i \frac{g_i c^2}{h} \int_0^\infty dp\, p\, \Gamma(M, E) f_p^{(i)}, \tag{44}$$

where $\Gamma(M, E)$ is the absorption coefficient. Using Equation (38) to write

$$\frac{dM}{dt} = -\frac{\alpha(M)}{M^2}, \tag{45}$$

we find a general form for $\alpha(M)$

$$\alpha(M) = \sum_i M^2 \frac{g_i}{h} \int_0^\infty dp\, p\, \Gamma(M, E) f_p^{(i)}. \tag{46}$$

Here, depending on the form of $\Gamma(M, E)$ we can calculate $\alpha(M)$ for a black body with temperature T_{BH}, as well as for a BH emission through the Hawking formula. Let us calculate both of them. For a black body we use $\Gamma(M, E)$ obtained in Equation (26). Inserting the dimensionless parameters

$$\widetilde{m}_i = \frac{8\pi GM}{\hbar c} m_i \quad , \quad x = \frac{8\pi GM}{\hbar c^2} p, \tag{47}$$

we can write

$$\begin{aligned} \frac{E_p}{kT} &= \frac{8\pi GM}{\hbar c^3} \sqrt{(m_i c^2)^2 + (pc)} \\ &= \sqrt{\widetilde{m}_i^2 + x^2}. \end{aligned} \tag{48}$$

Using

$$E_p = kT \sqrt{\widetilde{m}_i^2 + x^2} = c \frac{\hbar c^2}{8\pi GM} \sqrt{\widetilde{m}_i^2 + x^2}, \tag{49}$$

We obtain

$$\alpha(M) = \frac{\hbar c^4}{2^{11}\pi^5 G^2} \sum_i g_i \int_0^\infty dx\, x^2 \sqrt{\widetilde{m}_i^2 + x^2}\, f_p(\widetilde{m}_i, x), \tag{50}$$

where the sum is over all Standard Model particles. Figure 2 shows α as a function of the BH temperature (or BH mass). With $\alpha(M)$, we can obtain a better value of the BH lifetime. However, the integration cannot be done analytically due to the complicated depence of α on M. We must emphasize that Equation (50) is the α value using $\Gamma(M, E)$ of a black body emission with temperature T_{BH}.

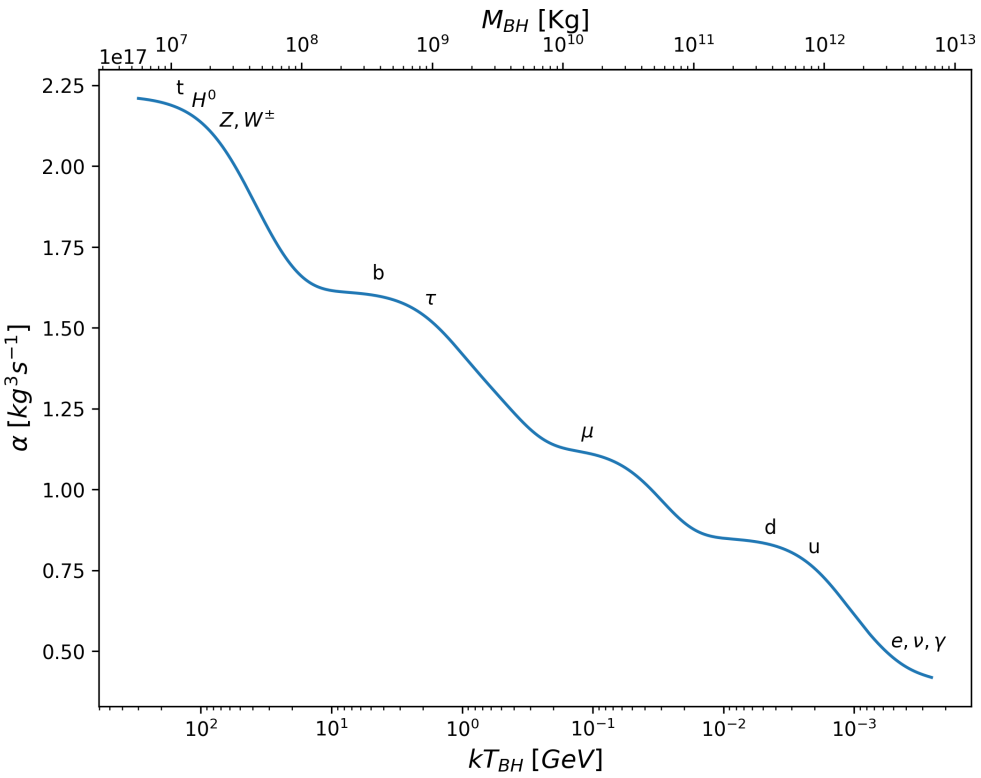

Figure 2: $\alpha(M)$ vs kT according to Equation (50). Each particle mass acts as a threshold. For m_i below kT_{BH}, the emission of particle i is supressed. As T_{BH} increases, new particles begin to contribute significantly to α. Notice that $\alpha(M)$ stabilizes at $\alpha_{SM} = 2.25 \times 10^{17}$ kg^{3}s^{-1}.

Now, let us calculate $\alpha(M)$ using Hawking's emission formula, which is the correct emission for a BH. This means that we must use the correct expression for the absorption coefficient. According to Equation (29) we use

$$\Gamma(M, E) \equiv \Gamma_{s_i}(M, E). \tag{51}$$

Inserting $\Gamma_{s_i}(M, E)$ in Equation (46)

$$\alpha(M) = \sum_i M^2 \frac{g_i}{h} \int_0^\infty dp\, p\, \Gamma_{s_i}(M, E) f_p^{(i)}, \tag{52}$$

and assuming that all emitted particles are massless ($E = pc$) we obtain

$$\alpha(M) = \frac{M^2}{c^2} \sum_i \int dE \frac{d\dot{N}_i}{dE} E, \tag{53}$$

where the sum is over all Standard Model particles for which the BH temperature has crossed the particle mass threshold. For a Schwarzschild BH, we use Equation (32) for the spectral emission rate. Then

$$\alpha(M) = \frac{M^2}{c^2} \sum_i \frac{g_i}{h} \int dE \, \frac{\Gamma_{s_i}(M, E)}{e^{E/kT} \pm 1} \, E, \tag{54}$$

but now we are forced to solve the last integral numerically, given that we do not have an analytical expression for the absorption coefficient $\Gamma_{s_i}(M, E)$. The function $\alpha(M)$ found in the literature using Equation (54) is shown in Figure 3.

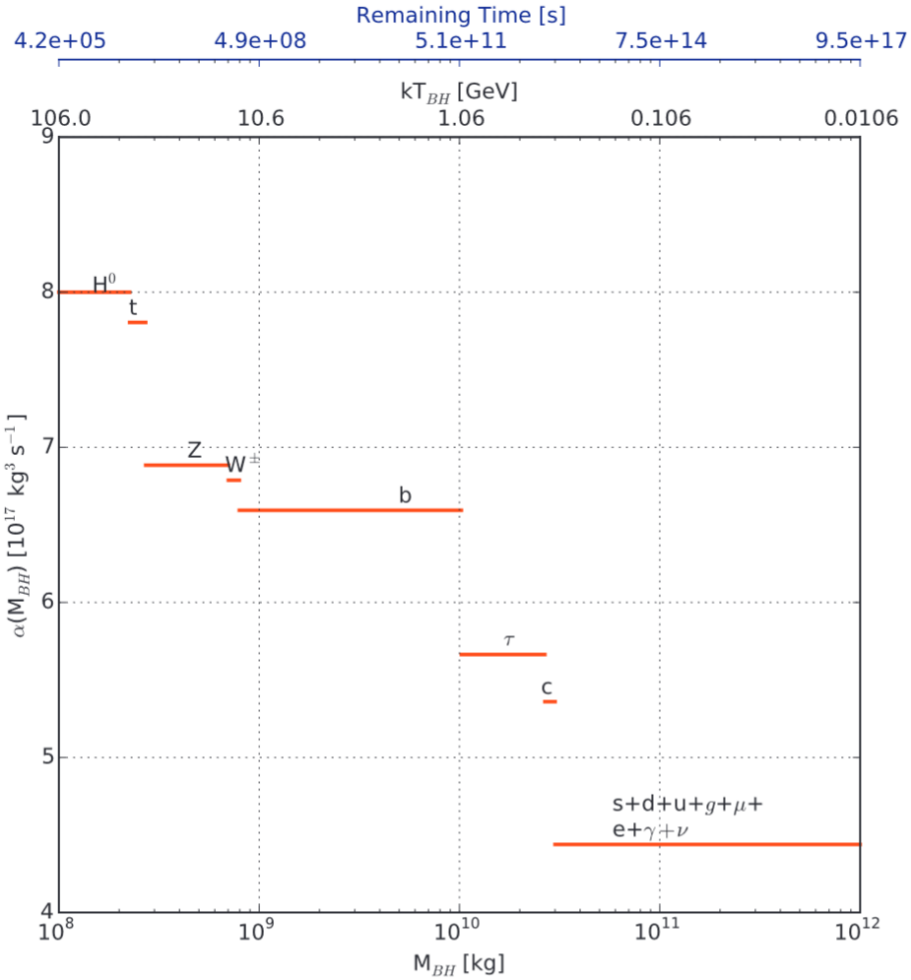

Figure 3: Value of $\alpha(M)$ obtained by Ref. [21]. When the BH has reached a temperature close to 10^2 GeV (a lifetime less than 5 days), all Standard Model particles are emitted, and the α value stabilizes at $\alpha_{SM} = 8.0 \times 10^{17}$ kg^{3}s^{-1}.

2 Primary spectrum

In order to calculate the time-integrated spectrum, we need to deal with the absorption coefficient $\Gamma_s(M, E)$. This function (also called greybody factor) measures the probability that particles could escape to infinity under the strong gravitational field of the BH, after being emitted in the event horizon vicinity. As the field of the emitted particle is decomposed in spherical harmonics, the $\Gamma_s(M, E)$ factor is obtained as the sum in all angular modes (see Ref. [16] for details). This function can only be calculated numerically. The greybody factor can be written as [21]

$$\Gamma_s(x) = 27 \left(\frac{x}{8\pi}\right)^2 \gamma_s(x) \quad , \quad x = \frac{E}{kT}. \tag{55}$$

Here, $\gamma_s(x)$ is obtained by numerical calculations. In the geometrical optics limit $x \gg 1$, $\gamma_s(x) \to 1$ for all species. Figure 4 shows $\gamma_s(x)$ for different spin s.

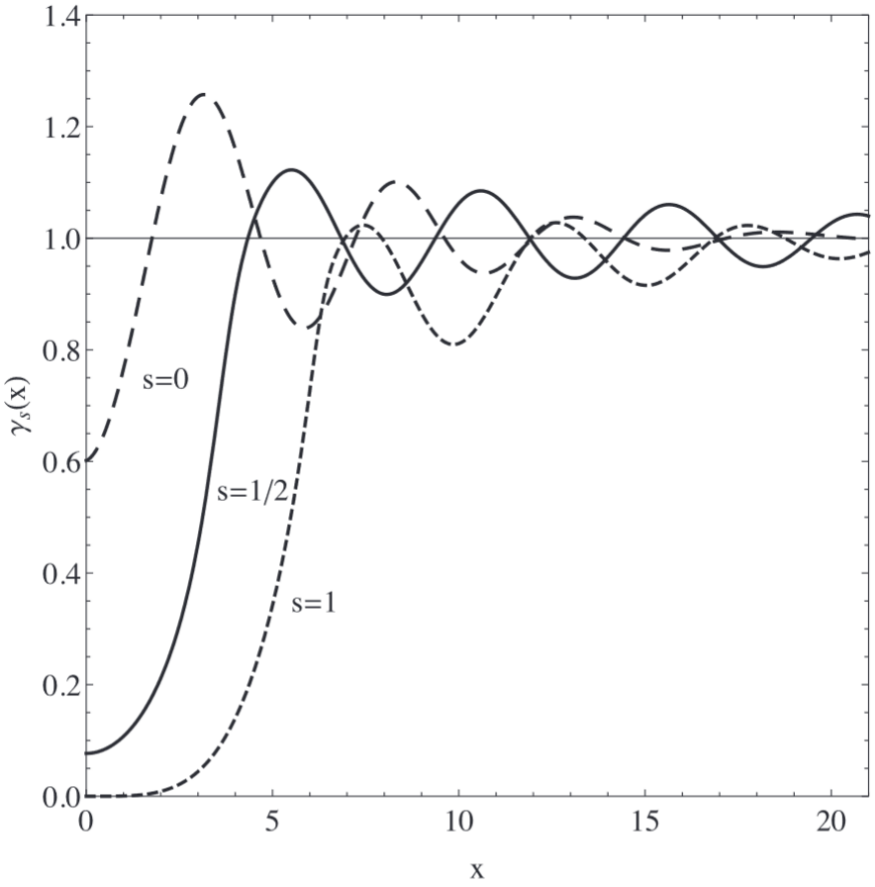

Figure 4: $\gamma(x)_s$ as a function of $x = E/kT$, for particles with spin $s = 0,\ 1/2,\ 1$.

One of the purposes of our work is to obtain an identifiable gamma ray signal of a PBH in the last months before total evaporation. To achieve this, we shall time-integrate the primary photon spectrum (directly emitted by the BH) along the PBH leftover lifetime. Then, we will obtain the total spectrum distribution of photons emitted from the present time until the PBH extinction. For a Schwarzschild BH, we use Equation (32) to write the spectral number of photons emitted by the PBH during its lifetime τ

$$\frac{dN_i}{dE} = \int_0^\tau dt \, \frac{d\dot{N}_i}{dE} = \frac{g_i}{h} \int_0^\tau dt \, \frac{\Gamma_{s_i}(x)}{e^x \pm 1}. \tag{56}$$

To solve this integral, we need x as function of t, i.e, the BH temperature as a function of time. To obtain this, we must solve the differential Equation (45) for the BH mass. This is a complicated task given the dependence of α on M. However, we can use the approximation $\alpha(M) \approx \alpha(M_0)$, where M_0 is the initial mass of a BH with lifetime τ, because most of the lifetime τ occurs in the regime where M is close to M_0. Then, as $\alpha(M_0)$ is constant, the approximate solution for Equation (45) is

$$M_0^3 \approx 3\,\alpha(M_0)\,\tau. \tag{57}$$

Actually, for a BH with mass less than $M_0 \approx 3 \times 10^8$ kg ($\tau \lesssim 130$ days), α is indeed fixed at the asymptotic value $\alpha_{SM} = 8.0 \times 10^{17}$ kg^{3}s^{-1} (see Figure 3). In this temperature regime, the BH radiates all Standard Model particles. Using Equation (2), we can write the BH temperature as a function of lifetime as

$$\frac{1}{kT} = \Lambda\,\tau^{1/3}, \tag{58}$$

where we have defined Λ as

$$\Lambda = \frac{8\pi G\,(3\alpha_{SM})^{1/3}}{\hbar c^3}. \tag{59}$$

Notice that Λ has units of GeV^{-1} s$^{-1/3}$. Then, we can write the adimensional variable x as a function of t:

$$x = \frac{E}{kT} = \Lambda E t^{1/3}. \tag{60}$$

Therefore, Equation (56) can be written as

$$\frac{dN_i}{dE} = \frac{3g_i}{\Lambda^3 h}\frac{1}{E^3}\int_0^{x_\tau} dx \, \frac{x^2\,\Gamma_s(x)}{e^x \pm 1}. \tag{61}$$

Here $x_\tau = E/kT_\tau = E\Lambda\tau^{1/3}$ corresponds to the beginning of a BH evaporation with a lifetime τ, while $x = 0$ corresponds to the instant when the BH evaporation has been completed ($kT_\tau \to \infty$). We should be careful to notice the last instants of evaporation ($\tau \leq t_{Pl} \sim 10^{-44}$ s) are in a regime where physics is not known (the Planck scale).

To solve the integral in Equation (61), we will use the approximations for greybody factors in the high and low energy limits, defined in Equations (30) and (31). In terms of x, we can write for $x \ll 1$ ($E \ll kT$)

$$\Gamma_s(x)_{x\ll 1} = \begin{cases} 16\left(\frac{x}{8\pi}\right)^2 & s = 0 \\ 2\left(\frac{x}{8\pi}\right)^2 & s = \frac{1}{2} \\ \frac{64}{3}\left(\frac{x}{8\pi}\right)^4 & s = 1 \\ \frac{256}{45}\left(\frac{x}{8\pi}\right)^6 & s = 2, \end{cases} \tag{62}$$

and for $x \gg 1$ ($E \gg kT$), $\Gamma_s(x)$ approaches to the geometrical optics limit

$$\Gamma(x)_{x\gg 1} = 27\left(\frac{x}{8\pi}\right)^2 \tag{63}$$

valid for all species.

2.1 The case $x_\tau \geq 1$

As the PBH evaporates, x decreases from x_τ to 0. If we consider energies E where initially $E \geq kT_\tau$, we will have $x_\tau > 1$ at early stages, and then as the PBH evaporates we will move to $x < 1$ until full evaporation. Thus, the integral over x covers regions where $x > 1$ and $x < 1$. For $x \gg 1$ ($E \gg kT_\tau$), we must use the high energy limit approximation for the greybody factor (Equation (63)), while for $x \ll 1$ ($E \ll kT_\tau$) we shall use the low energy expression for the greybody factor (Equation (62)). Then, the integral 61 can be written as

$$\frac{dN_i}{dE} = \frac{3g_i}{\Lambda^3 h}\frac{1}{E^3}\left(\int_0^{1-\delta} dx\,\frac{x^2\,\Gamma_s^{(l)}(x)}{e^x \pm 1} + \int_{1-\delta}^{1+\delta} dx\,\frac{x^2\,\Gamma_s(x)}{e^x \pm 1} + \int_{1+\delta}^{x_\tau} dx\,\frac{x^2\,\Gamma^{(h)}(x)}{e^x \pm 1}\right), \tag{64}$$

where the superscripts l and h hold for low and high energy limit respectively. The parameter $0 < \delta < 1$ is written to use the approximations of the greybody factors in their corresponding interval.

Also, it is convenient to write the greybody factor approximations as

$$\begin{aligned}\Gamma_s^{(l)}(x) &= C_s^{(l)} x^m \\ \Gamma^{(h)}(x) &= C^{(h)} x^2,\end{aligned} \tag{65}$$

where $m = 2, 2, 4, 6$ for $s = 0, 1/2, 1, 2$ respectively. We shall use the approximation $\delta = 0$. Then, Equation (64) takes the form

$$\frac{dN_i}{dE} \approx \frac{3g_i}{\Lambda^3 h}\frac{1}{E^3}\left(C_s^{(l)}\int_0^1 dx\,\frac{x^{m+2}}{e^x \pm 1} + C^{(h)}\int_1^{x_\tau} dx\,\frac{x^4}{e^x \pm 1}\right). \tag{66}$$

Using

$$\int_1^{x_\tau} dx\,\frac{x^4}{e^x \pm 1} = \int_0^{x_\tau} dx\,\frac{x^4}{e^x \pm 1} - \int_0^1 dx\,\frac{x^4}{e^x \pm 1}, \tag{67}$$

we can write

$$\frac{dN_i}{dE} \approx \frac{3g_i}{\Lambda^3 h}\frac{1}{E^3}\left(C_s^{(l)}\int_0^1 dx\,\frac{x^{m+2}}{e^x \pm 1} + C^{(h)}\int_0^{x_\tau} dx\,\frac{x^4}{e^x \pm 1} - C^{(h)}\int_0^1 dx\,\frac{x^4}{e^x \pm 1}\right). \tag{68}$$

These integrals have the general form

$$I_n(X, a) = \int_0^X ds\,\frac{s^n}{e^s + a} \quad \forall n \in \mathbb{N} \tag{69}$$

and $a = \pm 1$. This integral can be solved using the Method of Brackets. This is a powerful method of integration based on techniques used to evaluate Feynman diagrams [10]. This method solves definite integrals in one or several dimensions over the interval $[0, \infty[$. The procedure introduces the notion of a *bracket* and converts the integrand in a *series of brackets*. The method contains a small number of heuristic rules which transform the evaluation of an integral into the solution of a small linear system of equations. To solve the integral in Equation (69) with the Method of Brackets, we introduce the change of variable $y = s/(X - s)$ to set the integral limits at the interval $[0, \infty[$. The full calculations are shown in Ref. [9], where a new series expansion for this integral was found. Therefore, using the Method of Brackets, the integral $I_n(X, a)$ can be written as the following finite series:

$$I_n(X, a) = -\frac{\Gamma(n+1)}{a}\left(\mathbf{Li}_{n+1}(-a) - \sum_{k=0}^{n}\mathbf{Li}_{n+1-k}(-ae^{-X})\frac{X^k}{k!}\right). \tag{70}$$

Here, $\mathbf{Li}_n(z)$ is the polylogarithm function plotted in Figure 5

$$\mathbf{Li}_n(z) = \sum_{k=1}^{\infty} \frac{z^k}{k^n}, \tag{71}$$

for all complex n and z such that $|z| \leq 1$. Some important properties are

$$\mathbf{Li}_n(1) = \zeta(n) \quad , \quad \mathbf{Li}_n(-1) = -\eta(n) = -(1 - 2^{1-n})\,\zeta(n). \tag{72}$$

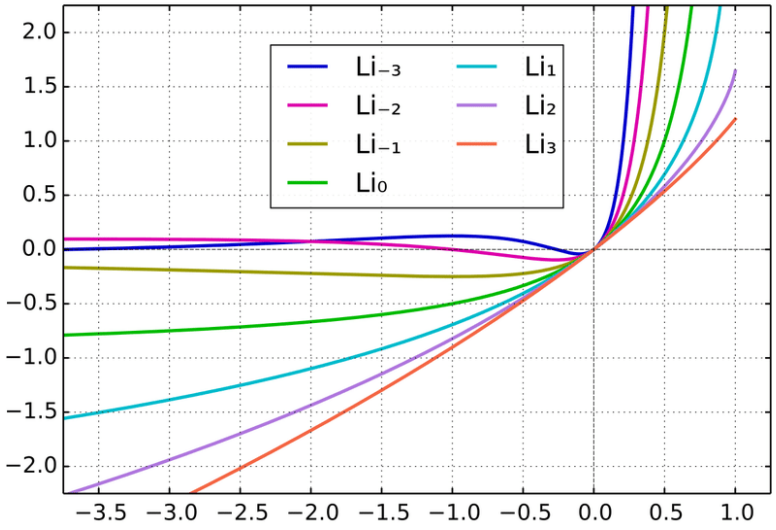

Figure 5: Plot of polylogarithm functions.

Therefore, the solution of Equation (68) by means of Equation (70) is

$$\frac{dN_i}{dE} \approx \frac{3g_i}{\Lambda^3 h}\frac{1}{E^3}\left(C_s^{(l)} I_{m+2}(1,\pm 1) + C^{(h)} I_4(x_\tau,\pm 1) - C^{(h)} I_4(1,\pm 1)\right). \tag{73}$$

Let us examine this solution for photons and quarks. For photons in the low energy limit (l) we set $m = 4$, $g_\gamma = 2$ and the coefficients C according to Equation (62). Then,

$$C_1^{(l)}\, I_6(1,-1) = \frac{\Gamma(7)}{192\pi^4}\left(\zeta(7) - \sum_{k=0}^{6} \mathbf{Li}_{7-k}(e^{-1})\,\frac{1}{k!}\right) \approx 10^{-6}$$

$$C^{(h)}\, I_4(1,-1) = \frac{27\,\Gamma(5)}{64\pi^2}\left(\zeta(5) - \sum_{k=0}^{4} \mathbf{Li}_{5-k}(e^{-1})\frac{1}{k!}\right) \approx 10^{-3} \tag{74}$$

$$C^{(h)}\, I_4(x_\tau,-1) = \frac{27\,\Gamma(5)}{64\pi^2}\left(\zeta(5) - \sum_{k=0}^{4} \mathbf{Li}_{5-k}(e^{-x_\tau})\,\frac{x_\tau^k}{k!}\right).$$

These results tell us that the contribution in the interval $x \in [0,1]$ is negligible. Using

$$\begin{aligned} \hbar &= 6.582 \times 10^{-25} \quad \text{GeVs} \\ \Lambda_{SM} &= \frac{8\pi G(3\alpha_{SM})^{1/3}}{\hbar c^3} \\ &= 1.264 \times 10^{-4} \quad \text{GeV}^{-1}\text{s}^{-1/3}, \end{aligned} \tag{75}$$

and inserting the expression for $C^{(h)}\, I_4(x_\tau,-1)$ in Equation (73), the approximate time-integrated spectrum of primary photons with energies $E \geq kT_\tau$ is:

$$\frac{dN_\gamma}{dE} \approx 7\times 10^{35}\left(\frac{E}{\text{GeV}}\right)^{-3}\left[\frac{27\,\Gamma(5)}{64\pi^2}\left(\zeta(5) - \sum_{k=0}^{4} \mathbf{Li}_{5-k}(e^{-E/kT_\tau})\,\frac{(E/kT_\tau)^k}{k!}\right)\right] \text{GeV}^{-1}, \tag{76}$$

where we have used $x_\tau = E/kT_\tau$. The expression inside square parentheses, approaches 1 for $E/kT_\tau \gtrsim 10$ as shown in Figure 6. This means that the time-integrated spectrum does not depend on the initial BH temperature kT_τ for photons with energies $E \gtrsim 10\,kT_\tau$. Notice that Refs. [15, 17, 21] consider the approximation

$$\frac{dN_\gamma}{dE} \approx 9\times 10^{35}\left(\frac{E}{\text{GeV}}\right)^{-3} \text{GeV}^{-1} \quad \text{for} \quad E \geq kT_\tau. \tag{77}$$

However as we just saw, this is not valid for all $E \geq kT$, but only for $E \gtrsim 10\,kT$. Indeed, in the range $E \sim kT$, the expression inside square parentheses is smaller than unity by a factor 10^{-3}: The spectrum is sizable only for $E \geq 10\,kT$. This is clearly different from the black body radiation.

Proceeding as in the previous case, the emission of a given flavor of quarks ($g_q = 12$) with energies $E > kT_\tau$ the time-integrated spectrum is:

$$\frac{dN_q}{dE} \approx 4 \times 10^{36} \left(\frac{E}{\text{GeV}}\right)^{-3} \left[\frac{27}{64\pi^2}\Gamma(5)\left(\frac{15}{16}\zeta(5) + \sum_{k=0}^{4} \mathbf{Li}_{5-k}(-e^{-E/kT_\tau})\frac{(E/kT_\tau)^k}{k!}\right)\right] \text{GeV}^{-1}. \tag{78}$$

The expression inside square parentheses is also plotted in Figure 6.

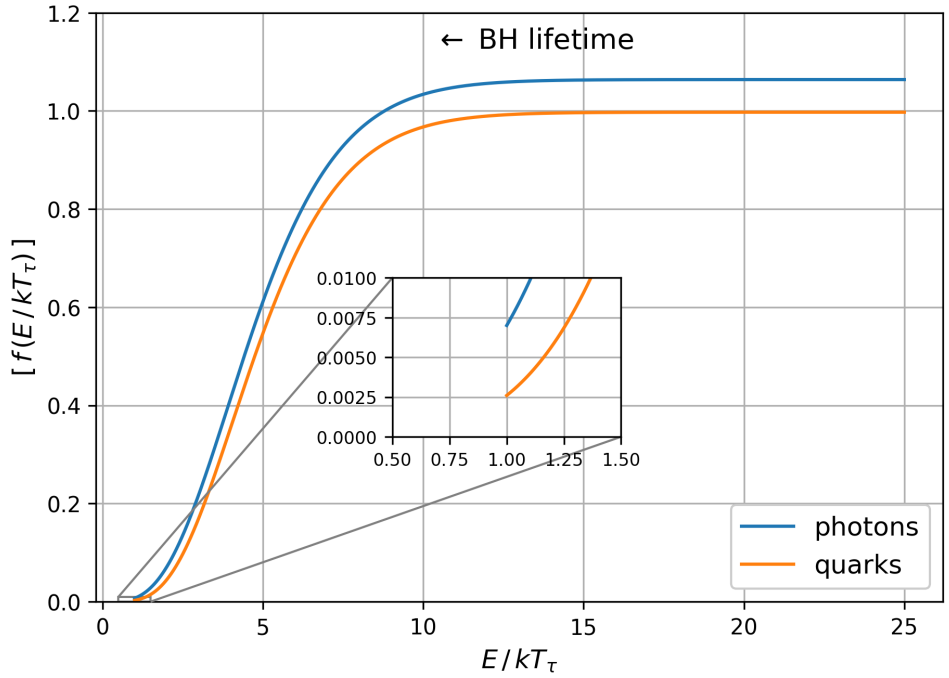

Figure 6: Contribution of the expressions inside square parentheses in Equations (76) and (78) for $x_\tau = E/kT_\tau \geq 1$.

2.2 The case $x_\tau < 1$

For particles with energies below the initial BH temperature ($E < kT_\tau$), we can time-integrate the spectrum using the approximation for the greybody factor in the low energy limit only (Equation (62)). This is because the condition $x < 1$ remains valid in the full integration range. Therefore, the time-integrated spectrum in this case (Equation (56)), can be written as

$$\frac{dN_i}{dE} \approx \frac{3g_i}{\Lambda^3 h}\frac{1}{E^3}\int_0^{x_\tau} dx\, \frac{x^2\,\Gamma_s^{(l)}(x)}{e^x \pm 1}. \tag{79}$$

Inserting the expression for $\Gamma_s^{(l)}(x)$ defined in Equation (65), this integral can be written as

$$\begin{aligned}\frac{dN_i}{dE} &\approx \frac{3g_i}{\Lambda^3 h}\frac{1}{E^3}\,C_s^{(l)}\int_0^{x_\tau} dx\,\frac{x^{m+2}}{e^x \pm 1}\\ &\approx \frac{3g_i}{\Lambda^3 h}\frac{1}{E^3}\,C_s^{(l)}\,I_{m+2}(x_\tau, \pm 1),\end{aligned} \tag{80}$$

where in the last line we used the integral definition Equation (69). According to Equation (62), for photons ($s = 1$) we set $m = 4$. Therefore, we need

$$C_1^{(l)}\,I_6(x_\tau, -1) = \frac{\Gamma(7)}{192\pi^4}\left(\zeta(7) - \sum_{k=0}^{6}\mathbf{Li}_{7-k}(e^{-x_\tau})\,\frac{x_\tau^k}{k!}\right). \tag{81}$$

Then, the time-integrated spectral emission of primary photons with energies $E < kT_\tau$ is:

$$\frac{dN_\gamma}{dE} \approx 7\times 10^{35}\,\left(\frac{E}{\mathrm{GeV}}\right)^{-3}\left[\frac{\Gamma(7)}{192\pi^4}\left(\zeta(7) - \sum_{k=0}^{6}\mathbf{Li}_{7-k}(e^{-E/kT_\tau})\,\frac{(E/kT_\tau)^k}{k!}\right)\right]\,\mathrm{GeV}^{-1}. \tag{82}$$

Similarly, for a given flavor of quarks ($s = 1/2$) we set $m = 2$ according Equation (62). Then, the time-integrated spectral emission of quarks with energies $E < kT_\tau$ is:

$$\frac{dN_q}{dE} \approx 4\times 10^{36}\,\left(\frac{E}{\mathrm{GeV}}\right)^{-3}\left[\frac{\Gamma(5)}{32\pi^2}\left(\frac{15}{16}\zeta(5) + \sum_{k=0}^{4}\mathbf{Li}_{5-k}(-e^{-E/kT_\tau})\,\frac{(E/kT_\tau)^k}{k!}\right)\right]\,\mathrm{GeV}^{-1}. \tag{83}$$

The contribution of the terms in the square parentheses of Equations (82) and (83) are shown in Figure 7.

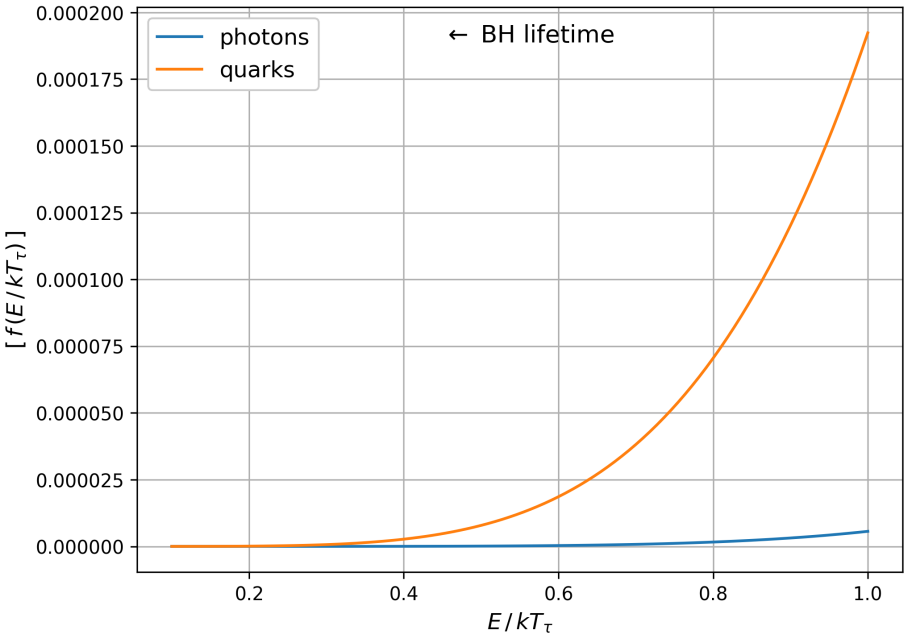

Figure 7: Contribution of the terms in the square parentheses in Equations (82) and (83) for $x_\tau \leq 1$.

Notice that this part of the spectrum ($E < kT_\tau$) becomes negligible towards the end of the BH evaporation. Indeed, the functions plotted in Figure 7 can explain why the emissions of particles with energies below the initial BH temperature are suppressed as we will see in Section 4.

Let us plot the time-integrated spectral emission of primary photons obtained in Equations (76) and (82) for several BH lifetimes below 100 seconds. To calculate the corresponding BH masses, we use Equation (57) with α_{SM}. Then

$$\begin{array}{lll} \tau = 100 \text{ s} & M = 6.2 \times 10^9 \text{ g} & kT_\tau = 1.7 \text{ TeV} \\ \tau = 10 \text{ s} & M = 2.9 \times 10^9 \text{ g} & kT_\tau = 3.7 \text{ TeV} \\ \tau = 1 \text{ s} & M = 1.3 \times 10^9 \text{ g} & kT_\tau = 8 \text{ TeV} \\ \tau = 0.1 \text{ s} & M = 6.2 \times 10^8 \text{ g} & kT_\tau = 17 \text{ TeV} \\ \tau = 0.01 \text{ s} & M = 2.9 \times 10^8 \text{ g} & kT_\tau = 37 \text{ TeV}, \end{array}$$

where we have used Equation (2) to compute the corresponding initial BH temperatures kT_τ. The time-integrated spectra of primary photons are shown in Figure 8

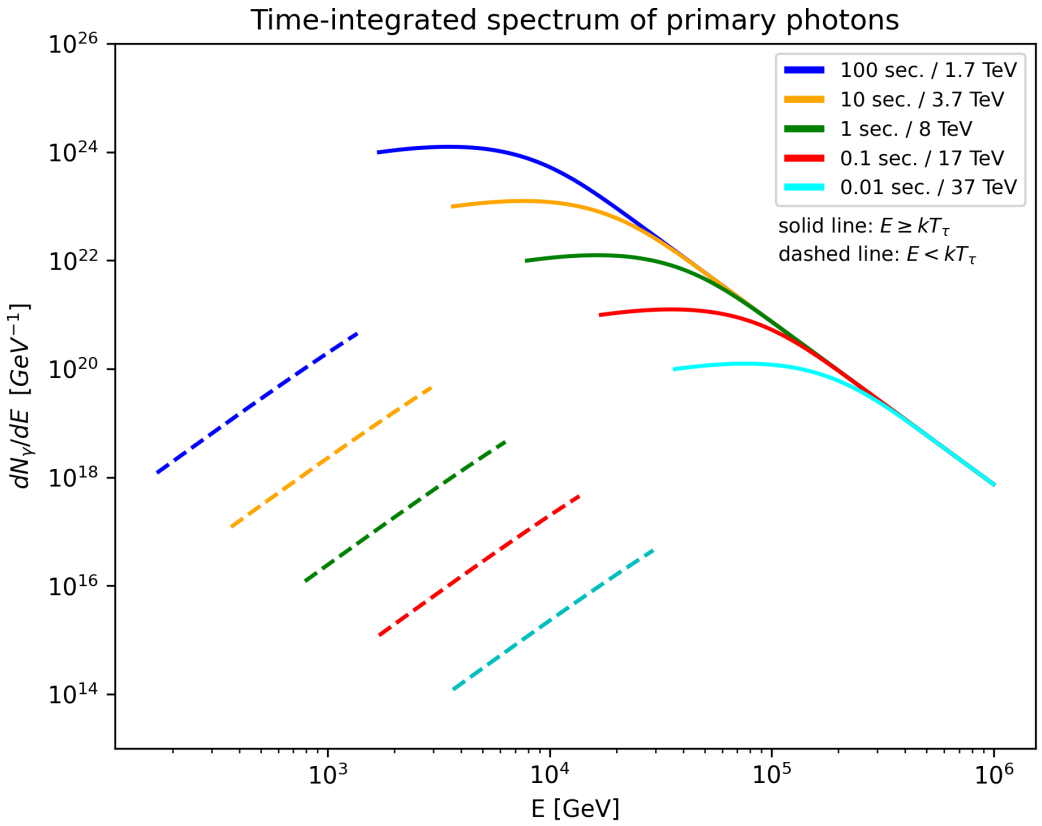

Figure 8: Time-integrated spectrum of primary photons for $x_\tau \geq 1$ ($E \geq kT_\tau$) and $x_\tau < 1$ ($E \leq kT_\tau$), as a function of the photon energy, for different BH lifetimes in the last 100 seconds before full BH evaporation.

In Figure 8, spectra in the low (dashed line) and high energy limit (solid line) seem to be shifted with respect to each other, i.e, we cannot extrapolate the dashed curves to the solid ones without a considerable slope change. This is not correct, as we shall see in the simulations chapter (Section 4). The relative energy shifting between both parts of the spectrum is given by an overestimation of primary photons in the regime $E \sim kT_\tau$. This overestimation comes from the approximate interval of $x = E/kT_\tau$ that we considered to do the integration using the greybody factor approximations (see Equation (66)).

3 Secondary spectrum

According to the Standard Model of particle phyisics, a distant observer of a BH evaporating should detect the following particles: $\gamma, \nu, e^{\pm}, p^{\pm}$. Any other particle will decay into these species. As we are interested in photon detection, the main factory that produces them, apart from those directly emitted by the BH, is the π^0 decay through the process $\pi^0 \to \gamma\gamma$, that occurs with a 98% of the cases [22]. These photons constitute the secondary photon spectrum of a BH evaporation.

When kT_{BH} reaches the quark-gluon confinement energy scale ($\Lambda_{QCD} \sim 200 - 300$ MeV), the BH emits free quarks and gluons. When this happens, practically all of them will fragment into all kinds of hadrons such as neutrons, protons, pions, kaons, B mesons, D mesons, etc. This phenomenon is similar to the jets produced in the high-energy collisions at colliders. Nevertheless, through the different decay modes, these hadrons will end as up decaying into the stable species mentioned above. For example, let us examine the $K^{\pm}$ meson. The main decay channel is the leptonic $K^{\pm} \to \mu^{\pm}\nu_{\mu}$ that occurs with a 64% of the cases, and the non-leptonic $K^{\pm} \to \pi^{\pm}\pi^0$ with a 20% of the cases [22]. Both modes, after the $\mu^{\pm}$ and $\pi^{\pm,0}$ decays, will end up in electrons, neutrinos and photons. The estimation of π production is a complicated task, given the complexity of the quark hadronization phenomenon. This calculation is usually obtained using programs based on Monte Carlo simulations [5, 19]. However, using some crude approximations, we can calculate the π emission analytically, and then the secondary photon emission. The purpose of this section is to obtain the time-integrated spectrum of the secondary photons from the π^0 decay to complement the photon signal from a BH evaporation.

3.1 Fragmentation function

To estimate the π production, we shall use an empirical fragmentation function usually used in the literature [11, 21]

$$D_{h/q}(z) = \frac{15}{16}\frac{(1-z)^2}{z^{3/2}} \quad , \quad z = \frac{E_h}{E}. \tag{84}$$

This function represents the probability that a quark q with energy E fragments into a hadron h with energy E_h. Here, z is the quotient between the energy E_h carried by the resultant hadron and the energy E of initial quark. The function $D_{h/q}(z)$ is shown in Figure 9. This

function has the following properties:

$$\sum_q \int_0^1 dz\ D_{h/q}(z) = n_h$$
$$\sum_h \int_0^1 dz\ zD_{h/q}(z) = 1, \tag{85}$$

where the sum over q is the contribution of all parent quark flavors. The first property expresses that the average number of hadrons of type h, is equivalent to the sum of all probabilities to obtain a hadron h along all possible fractions of energy of the parent quarks. The second property states that the sum of all energies of hadrons of type h is equivalent to the energy of the parent quark.

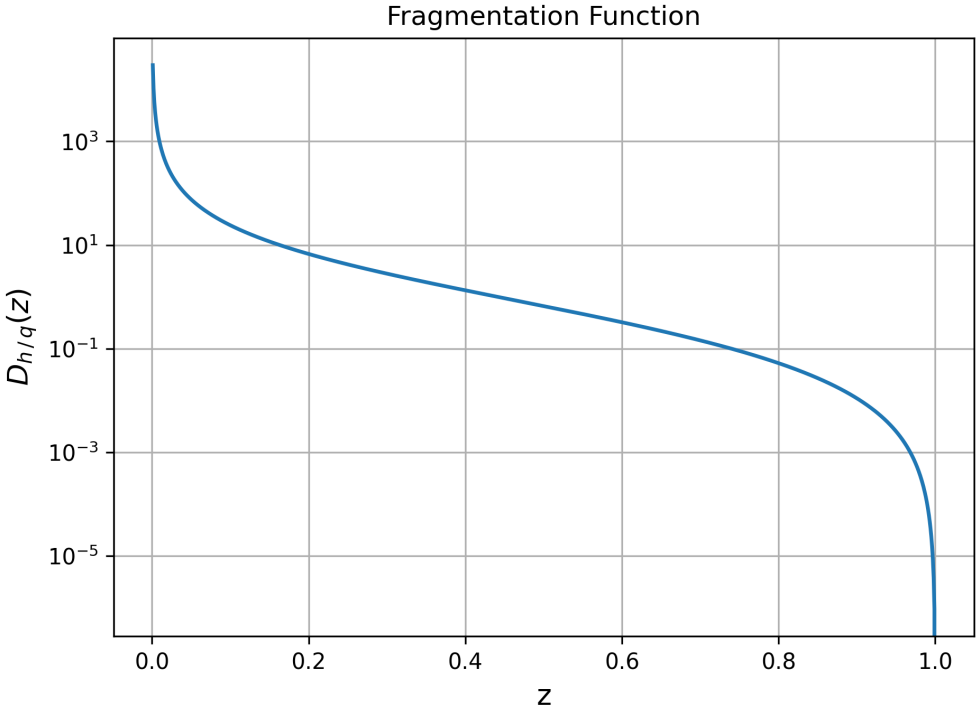

Figure 9: $D_{h/q}(z)$ as a function of $z = E_h/E$ defined in Equation (84).

The quark spectral emission rate of a given flavor quark q, according Hawking's emission formula (Equation (32)) is:

$$\frac{d\dot{N}_q}{dE} = \frac{g_q}{h}\frac{\Gamma_{1/2}(x)}{e^x + 1}, \tag{86}$$

where $x = E/kT_\tau$ and g_q is the number of degrees of freedom. Notice that we have assumed massless quarks. Proceeding as we did for the primary spectrum, we shall use the approxi-

mations of the greybody factors in the low and high energy limits defined in Equations (62) and (63). Using $g_q = 12$, the quark spectral emission rate can be written as:

$$\frac{d\dot{N}_q}{dE} = \begin{cases} \frac{3}{16\pi^3\hbar}\frac{x^2}{e^x+1} \equiv C^{(l)} f(x)\ , & E \ll kT \\ \\ \frac{81}{32\pi^3\hbar}\frac{x^2}{e^x+1} \equiv C^{(h)} f(x)\ , & E \gg kT, \end{cases} \tag{87}$$

where

$$f(x) \equiv \frac{x^2}{e^x + 1}. \tag{88}$$

A pion is a meson (a boson made of two quarks) composed of u, d quarks. As a consequence, the pion spectral emission rate due to the u, d hadronization can be obtained through the product of the u, d quark spectral emission rate (Equation (87)) and the probability that they get hadronized into pions, i.e, the $D_{\pi/q}(z)$ fragmentation function (Equation (84)). As the resultant pion carries a fraction of the quark energy $E_\pi = zE$, the pion spectral emission rate can be written as:

$$\frac{d\dot{N}_\pi}{dE_\pi} = \sum_{q=u,d} \int_0^\infty dE \int_0^1 dz\, \frac{d\dot{N}_q}{dE}\, D_{\pi/q}(z)\, \delta(E_\pi - zE). \tag{89}$$

Here, the sum accounts for all quark flavors, but in the case of c, s, t, b quarks, we must calculate their respective decays to the u, d quarks.

3.2 Hadronization from u and d quarks

Let us calculate the hadronization into pions due to the u, d quarks that are directly emitted by the BH. For this purpose, let us count the number of particles per unit time (hereafter the number) emitted in a certain range of energy. The number of u quarks emitted in the energy range $[E_u, E_u + dE_u]$ is $d\dot{N}_u$. Similarly, the number of d quarks emitted in the energy range $[E_d, E_d + dE_d]$ is $d\dot{N}_d$. Then,

$$d\dot{N}_u = d\dot{N}_d. \tag{90}$$

This means that the quark hadronization into pions given the primary u and d quarks are equal. Therefore, the fragmentation functions for each flavor satisfy

$$D_{\pi/u}(z) = D_{\pi/\bar{u}}(z) = D_{\pi/d}(z) = D_{\pi/\bar{d}}(z) \quad , \quad z = \frac{E_\pi}{E}, \tag{91}$$

where E is the energy of the u or d quark. Then, using Equation (89) the quark hadronization into pions given the primary u, d quarks can be written as:

$$\begin{aligned}\frac{d\dot{N}_\pi}{dE_\pi}^{(u,d)} &= 2\int_0^\infty dE\,\frac{d\dot{N}_u}{dE}\int_0^1 dz\,D_{\pi/u}(z)\,\delta(z\,E-E_\pi)\\ &= 2\int_0^\infty dE\,\frac{d\dot{N}_u}{dE}\,\frac{1}{E}\,D_{\pi/u}\left(\frac{E_\pi}{E}\right).\end{aligned} \tag{92}$$

Using the change of variable $x = E/kT$, and inserting Equation (87)

$$\begin{aligned}\frac{d\dot{N}_\pi}{dE_\pi}^{(u,d)} &= 2\left(C^{(l)}\int_0^1 dx\,\frac{f(x)}{x}+C^{(h)}\int_1^\infty dx\,\frac{f(x)}{x}\right)D_{\pi/u}\left(\frac{E_\pi}{E}\right)\\ &= 2\left((C^{(l)}-C^{(h)})\int_0^1 dx\,\frac{f(x)}{x}\,D_{\pi/u}\left(\frac{E_\pi}{x\,kT}\right)+C^{(h)}\int_0^\infty dx\,\frac{f(x)}{x}\,D_{\pi/u}\left(\frac{E_\pi}{x\,kT}\right)\right).\end{aligned} \tag{93}$$

Notice that for the integration, we have used the same approximation of Section 2.1 (Equation (66)). Therefore, the integral on the interval $[0, 1]$ gives a negligible contribution. Then,

$$\frac{d\dot{N}_\pi}{dE_\pi}^{(u,d)} \approx 2\,\frac{15}{16}\,C^{(h)}\int_0^\infty dx\,\frac{f(x)}{x}\left[\left(\frac{x\,kT}{E_\pi}\right)^{3/2}-2\left(\frac{x\,kT}{E_\pi}\right)^{1/2}+\left(\frac{E_\pi}{x\,kT}\right)^{1/2}\right]. \tag{94}$$

Inserting the value for $C^{(h)}$ defined in Equation (87) and use $1/3$ for neutral pions, the π^0 spectral emission rate, given the primary u, d quarks is:

$$\frac{d\dot{N}_{\pi^0}}{dE_{\pi^0}}^{(u,d)} \approx \frac{1}{3}\left(\frac{1215}{256\pi^3\hbar}\right)\left[I(7)\left(\frac{kT}{E_{\pi^0}}\right)^{3/2}-2\,I(5)\left(\frac{kT}{E_{\pi^0}}\right)^{1/2}+I(3)\left(\frac{E_{\pi^0}}{kT}\right)^{1/2}\right], \tag{95}$$

where we have used the identity

$$I(s)=\int_0^\infty dx\,\frac{x^{s/2-1}}{e^x+1}=\Gamma(s/2)\eta(s/2)=\Gamma(s/2)(1-2^{1-s/2})\zeta(s/2). \tag{96}$$

We must warn that the contribution of $D_{\pi/\bar{u}}$ and $D_{\pi/\bar{d}}$ are already included in the degrees of freedom of $d\dot{N}/dE$. It is remarkable that the π^0 spectral emission rate depends on E and kT only through the rate E/kT, just as in the primary spectrum.

3.3 Heavy quark hadronization

In order to estimate the pion production due to c, s, b, t quark hadronization, we must estimate the u, d production through the decay of the heavy quarks. However, given the complexity of the phenomenon, we shall use some rude approximations:

1. The quark mixing matrix is diagonal, so the flavor change is either in the same generation or to the nearest generation. Note that in the t quark decay, the W^+ boson is real (see Figure 10).
2. We ignore the contribution of the W^+.
3. The production of quarks is by primary emission (directly emitted from the BH) and by the flavor quark changing. Any other mode of production is ignored.
4. We do not consider the leptonic mode $q \to q'\, l^{\pm}\, \nu$.
5. All quarks hadronize into pions instead any other hadron.
6. Energy equipartition for each decay process. This means that for each process shown in Figure 10, the final particles have the same energy.

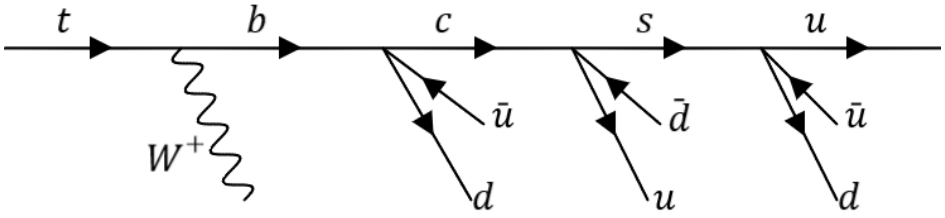

Figure 10: Approximate model of secondary u, d quark production given the flavor quark changing.

For convenience, we shall refer to u, d quarks as u-type quarks, because their hadronization into pions are equal (see Section 3.2). For a q quark with energy E_q that decays in n u-type quarks, the energy of these u-type quarks will be E_q/n. For example, the process $s \to u + \bar{u} + d$, the s quark with energy E_s decay in three u-type quarks such that each one has energy $E_s/3$. Then, the number of u-type quarks in the energy interval $[E_u, E_u + dE_u]$ is related to the number of s quarks in the energy interval $[E_s, E_s + dE_s]$ through

$$\begin{aligned} d\dot{N}_u(E_u) &= 3\, d\dot{N}_s(E_s) \\ &= 3\, d\dot{N}_s(3E_u). \end{aligned} \tag{97}$$

According to Equation (94), quark hadronization into pions comes from the term with the coefficient $C^{(h)}$ only, i.e, $C^{(l)}$ is neglected. Then, using Equation (87) we can write

$$d\dot{N}_s(3E_u) = C^{(h)} \frac{(3E_u/kT)^2}{e^{3E_u/kT}+1} 3dE_u. \tag{98}$$

Inserting Equation (98) in Equation (97), we obtain the spectral emission rate for the secondary u-type quarks coming from s quark decay

$$\Rightarrow \frac{d\dot{N}_{u/s}}{dE_u} = 9\, C^{(h)} \frac{(3E_u/kT)^2}{e^{3E_u/kT}+1}. \tag{99}$$

Now, inserting this result in Equation (89) we can obtain an approximation to the s quark hadronization into pions. To obtain the complete quark hadronization into pions, we must estimate the u-type quark production for each quark decay process of figure Figure 10. Given the extension, the full calculation is available in the appendix in Section 9.

According to our calculations (available in the appendix in Section 9), the approximate spectral emission rate of neutral pions from the hadronization of all quark flavors is:

$$\frac{d\dot{N}_{\pi^0}}{dE_{\pi^0}} = \frac{405}{512\pi^3\hbar} \left[I(7)\, F_{-3/2}\left(\frac{E_{\pi^0}}{kT}\right) - 2I(5)\, F_{-1/2}\left(\frac{E_{\pi^0}}{kT}\right) + I(3)\, F_{1/2}\left(\frac{E_{\pi^0}}{kT}\right) \right], \tag{100}$$

where we have defined $F_m(E/kT)$ as

$$\begin{aligned} F_m\left(\frac{E}{kT}\right) = 2\left(\frac{E}{kT}\right)^m + 21\left(\frac{3E}{kT}\right)^m + 12\left(\frac{6E}{kT}\right)^m + 45\left(\frac{9E}{kT}\right)^m \\ + 36\left(\frac{18E}{kT}\right)^m + 81\left(\frac{27E}{kT}\right)^m + 162\left(\frac{54E}{kT}\right)^m. \end{aligned} \tag{101}$$

This spectrum is shown in Figure 11.

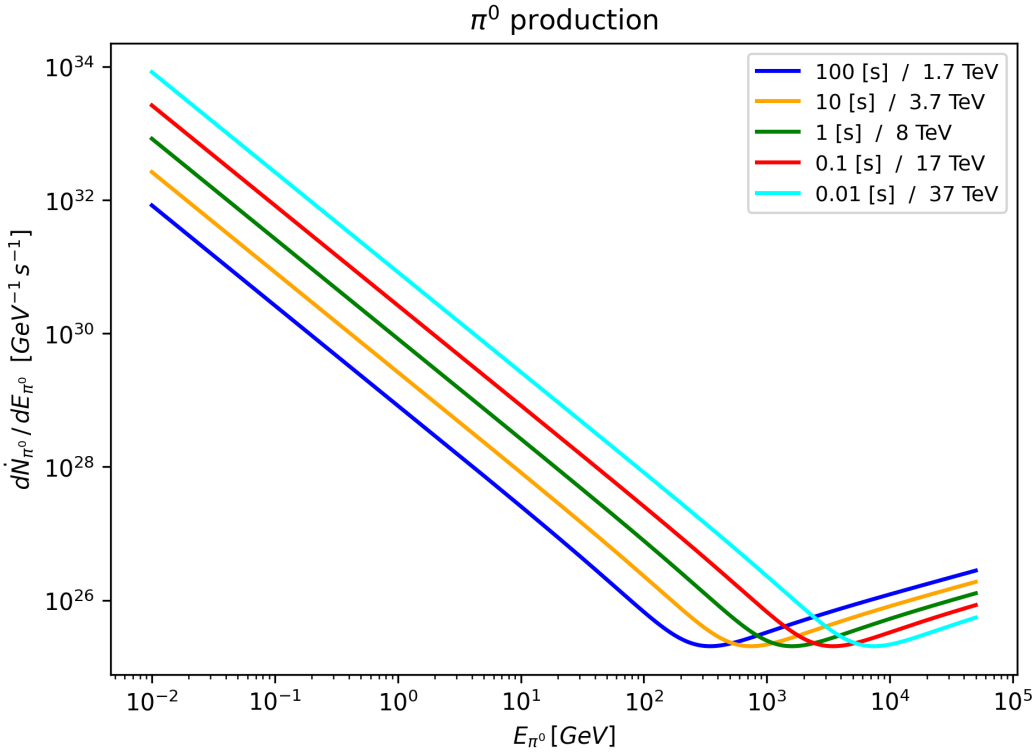

Figure 11: Spectral emission rate of neutral pions as a function of the pion energy, due to quarks hadronization, for different BH lifetimes in the last 100 seconds before full BH evaporation.

3.4 $\pi^0 \to \gamma\gamma$

The main source of secondary photons is the π^0 decay. Now that we have an estimation of the π^0 production, we can calculate the secondary photon spectrum from the $\pi^0 \to \gamma\gamma$ process. In the π^0 rest frame, both photons have equal energy and opposite momenta. In the detector frame, the pion is moving towards the detector with velocity v_π and energy $E_{\pi^0} = \gamma m_\pi c^2$, where γ is the Lorentz factor and m_π is the π^0 mass (see Figure 12). In this reference frame, the photons have energy E' as a function of the θ angle according to:

$$\begin{aligned} E'_{1,2} &= \gamma \frac{m_\pi c^2}{2} (1 \pm \beta \cos\theta) \\ \gamma &= \frac{1}{\sqrt{1-\beta^2}} \ , \ \beta = \frac{v_\pi}{c}. \end{aligned} \tag{102}$$

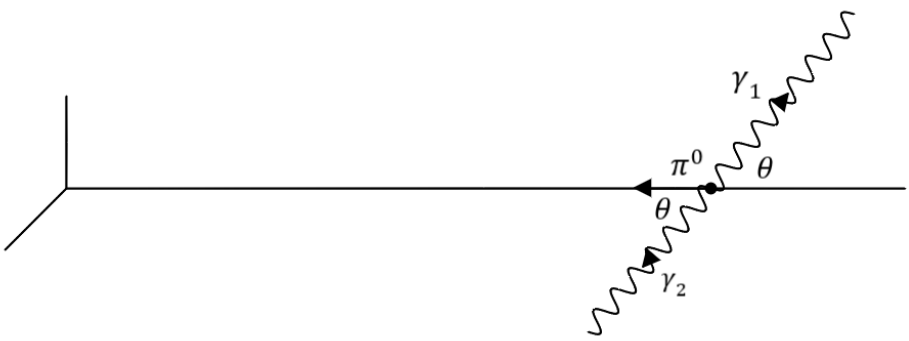

Figure 12: Diagram of $\pi^0 \to \gamma\gamma$ viewed from the detector frame.

As we have done rough approximations to estimate the π^0 production, we shall assume that both photons go forward with the same energy $E_\gamma = E_{\pi^0}/2$. In this picture, the number of photons in the energy interval $[E_\gamma, E_\gamma + dE_\gamma]$ is related to the number of π^0 in the energy interval $[E_{\pi^0}, E_{\pi^0} + dE_{\pi^0}]$ through

$$d\dot{N}_{\gamma/\pi^0}(E_\gamma) = 2\, d\dot{N}_{\pi^0}(2E_\gamma) \quad , \quad E_\gamma = \frac{E_{\pi^0}}{2}, \tag{103}$$

where

$$\begin{aligned} d\dot{N}_{\pi^0}(2E_\gamma) &= \frac{d\dot{N}_{\pi^0}}{dE_{\pi^0}}(2E_\gamma)\, dE_{\pi^0} \\ &= 2\,\frac{d\dot{N}_{\pi^0}}{dE_{\pi^0}}(2E_\gamma)\, dE_\gamma \\ \Rightarrow \frac{d\dot{N}_\gamma}{dE_\gamma} &= 4\frac{d\dot{N}_{\pi^0}}{dE_{\pi^0}}(2E_\gamma). \end{aligned} \tag{104}$$

Using Equation (100) we obtain the spectral emission rate of secondary photons due to π^0 decay

$$\frac{d\dot{N}_{\gamma/\pi^0}}{dE_\gamma} = \frac{405}{128\pi^3\hbar}\left[I(7)\, F_{-3/2}\left(\frac{2E_\gamma}{kT}\right) - 2I(5)\, F_{-1/2}\left(\frac{2E_\gamma}{kT}\right) + I(3)\, F_{1/2}\left(\frac{2E_\gamma}{kT}\right)\right], \tag{105}$$

where the $F_m(2E_\gamma/kT)$ function is read from Equation (101). This spectrum is plotted in Figure 13.

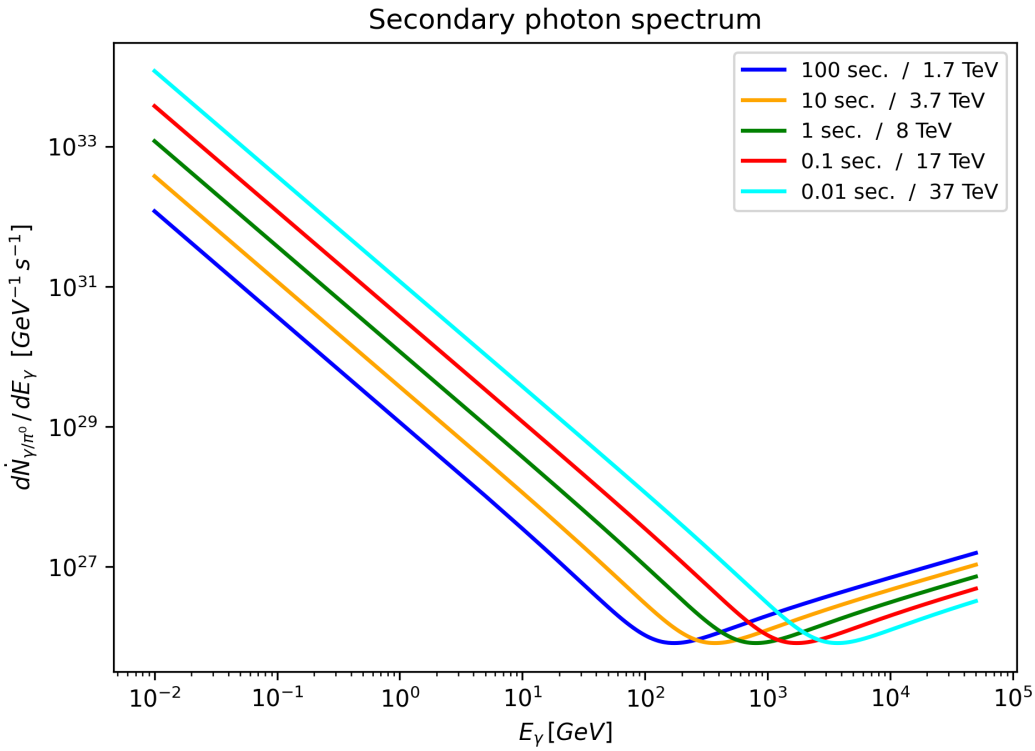

Figure 13: Spectral emission rate of secondary photons (due to the π^0 decay) as a function of the photon energy, for different BH lifetimes in the last 100 seconds before full BH evaporation.

To obtain the complete photon signal, we need to add to Equations (76) and (82), the time-integrated spectral emission of secondary photons (Equation (105)) along the BH lifetime. As we proceed in Section 2

$$\frac{dN_{\gamma/\pi^0}}{dE_\gamma} = \int_0^\tau dt\, \frac{d\dot{N}_{\gamma/\pi^0}}{dE_\gamma}. \tag{106}$$

Let us write Equation (105) in the following abbreviated way:

$$\frac{d\dot{N}_{\gamma/\pi^0}}{dE_\gamma} \propto \sum_{\{m\}} \left(\frac{n\,2E_\gamma}{kT}\right)^m, \tag{107}$$

where n is a fixed number for each term of $F_m(E/kT)$ function according to Equation (101). As usual, we use the change of variable $x = E_\gamma/kT = \Lambda E_\gamma t^{1/3}$, where Λ is defined in

Equation (59) (see Section 2 for the details). Then, Equation (106) can be written as

$$\begin{aligned}\frac{d\dot{N}_{\gamma/\pi^0}}{dE_\gamma} &\propto \sum_{\{m\}} \int_0^\tau dt \left(\frac{n\,2E_\gamma}{kT}\right)^m \\ &\propto \sum_{\{m\}} \frac{3\,(2n)^m}{(\Lambda E)^3} \int_0^{x_\tau} dx\, x^{2+m} \\ &\propto \sum_{\{m\}} \frac{3\,(2n)^m}{(\Lambda E)^3} \frac{x_\tau^{m+3}}{m+3}.\end{aligned} \tag{108}$$

Replacing the corresponding terms of $F_m(E/kT)$ with their respective m and n values (see Equation (101)), we found that the time-integrated spectrum of secondary photons due to the π^0 decay is:

$$\frac{dN_{\gamma/\pi^0}}{dE_\gamma} = \frac{1215}{32\pi^3\Lambda^3\hbar}\left[\frac{I(7)}{3}F_{-3/2}(2E_\gamma\,kT) - \frac{2I(5)}{5}(kT)^{-5/2}F_{-1/2}(2E_\gamma) + \frac{I(3)}{7}(kT)^{-7/2}F_{1/2}(2E_\gamma)\right] \tag{109}$$

where F_m functions are read from Equation (101). The spectrum is shown in Figure 14.

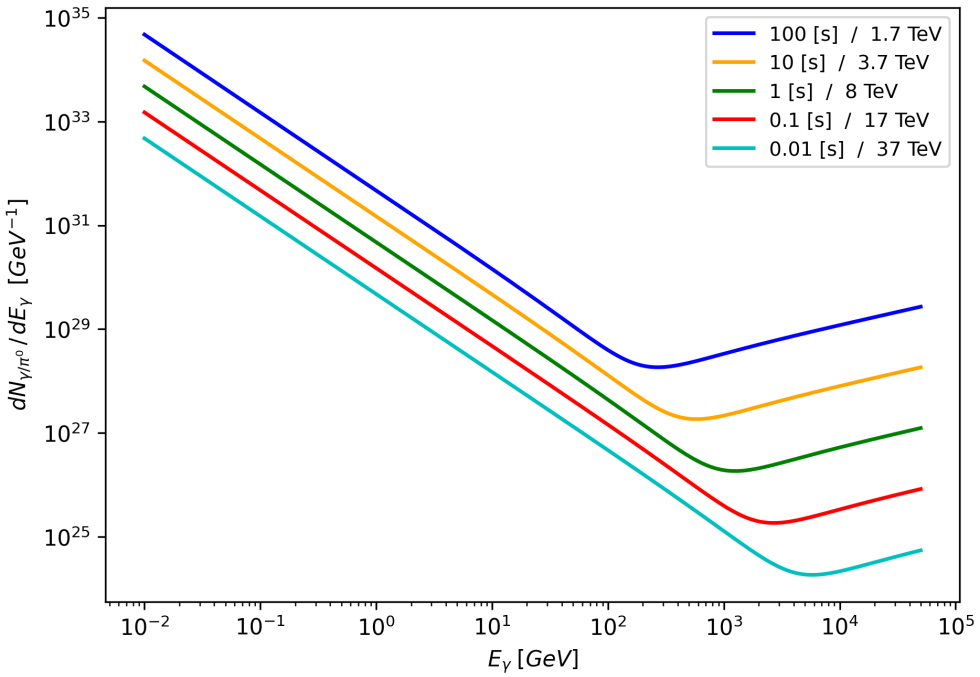

Figure 14: Time-integrated spectrum of secondary photons as a function of the photon energy, for different BH lifetimes in the last 100 seconds before full BH evaporation.

3.5 Photon spectrum discussion

We have calculated the time-integrated spectrum for photons which are directly emitted by the BH (primary photons) and for those coming from the π^0 decay after quarks hadronization (secondary photons) using some approximations. Both mecanisms contribute to the total photon spectrum of the BH evaporation phenomenon. We know *a priori* that the time-integrated photon spectrum is dominated by secondary photons at low energies $E_\gamma < kT_\tau$, and dominated by primary photons at high energies $E_\gamma \geq kT_\tau$ [15, 17, 21]. However, from Figures (8) and (14), the reader cannotice that secondary photons dominate even in the high energy limit ($E_\gamma \geq kT_\tau$). The reason of this is an overestimation of high energy pions. As a consequence, the secondary photon spectrum is overestimated, exceeding the primary photon spectrum. This overestimation is caused by the crude approximations that we have used to calculate the quark hadronization process. We are replacing the leptonic mode of $W^\pm$ decay for the hadronization into pions. Secondly, we are replacing the hadronization into D, B, K, etc., mesons by the hadronization into high energetic pions only. Additionally, the term $I(3)F_{1/2}(E_{\pi^0}/kT)$ in Equation (100) becomes dominant for $E_{\pi^0} \geq kT_\tau$. This is due to the form of the fragmentation function (Equation (84)). An alternative to reduce the photon overestimation is to aproximate the $F_m(E/kT)$ function of the secondary spectrum (Equation (109))

$$F_m\left(\frac{E}{kT}\right) \approx 2\left(\frac{E}{kT}\right)^m, \tag{110}$$

such that the spectral emission rate of secondary photons (Equation (105)) is

$$\frac{d\dot{N}_{\gamma/\pi^0}}{dE_\gamma} \approx \frac{405}{64\pi^3\hbar}\left[I(7)\left(\frac{2E_\gamma}{kT}\right)^{-3/2} - 2I(5)\left(\frac{2E_\gamma}{kT}\right)^{-1/2} + I(3)\left(\frac{2E_\gamma}{kT}\right)^{1/2}\right], \tag{111}$$

and the time-integrated spectrum (Equation (109))

$$\frac{dN_{\gamma/\pi^0}}{dE_\gamma} \approx \frac{1215}{16\pi^3\Lambda^3\hbar}\left[\frac{I(7)}{3}\left(2E_\gamma\, kT\right)^{-3/2} - \frac{2I(5)}{5}(kT)^{-5/2}\left(2E_\gamma\right)^{-1/2} + \frac{I(3)}{7}(kT)^{-7/2}\left(2E_\gamma\right)^{1/2}\right]. \tag{112}$$

Furthermore, taking the leading term of Equation (112) we obtain

$$\begin{aligned}\frac{dN_{\gamma/\pi^0}}{dE_\gamma} &\approx \frac{1215}{16\pi^3\Lambda^3\hbar}\frac{I(7)}{3}\left(2E_\gamma\, kT\right)^{-3/2} \\ &\approx 2\times 10^{36}\left(\frac{E_\gamma}{\mathrm{GeV}}\right)^{-3/2}\left(\frac{kT}{\mathrm{GeV}}\right)^{-3/2} \quad \mathrm{GeV}^{-1}.\end{aligned} \tag{113}$$

This approximation decreases the time-integrated secondary spectrum in the high energy limit ($E_\gamma \geq kT$) allowing that the primary spectrum dominates slightly in this energy limit. Using Equations (76) and (113) we can write the total time-integrated photon spectrum of a BH evaporation as

$$\frac{dN_\gamma}{dE_\gamma} \approx 7 \times 10^{35} \begin{cases} \left(\frac{E_\gamma}{\mathrm{GeV}}\right)^{-3} \mathrm{GeV}^{-1} & \text{for} \quad E_\gamma \gtrsim 10\, kT_\tau \quad \text{Primary} \\ 3 \left(\frac{E_\gamma}{\mathrm{GeV}} \frac{kT_\tau}{\mathrm{GeV}}\right)^{-3/2} \mathrm{GeV}^{-1} & \text{for} \quad E_\gamma < kT_\tau \quad \text{Secondary}, \end{cases} \tag{114}$$

which is shown in Figure 15. This result differs slightly from the total spectrum found in Refs. [15, 17, 21] which is

$$\frac{dN_\gamma}{dE_\gamma} \approx 9 \times 10^{35} \begin{cases} \left(\frac{E_\gamma}{\mathrm{GeV}}\right)^{-3} \mathrm{GeV}^{-1} & \text{for} \quad E_\gamma \geq kT_\tau \quad \text{Primary} \\ \left(\frac{E_\gamma}{\mathrm{GeV}} \frac{kT_\tau}{\mathrm{GeV}}\right)^{-3/2} \mathrm{GeV}^{-1} & \text{for} \quad E_\gamma < kT_\tau \quad \text{Secondary}. \end{cases} \tag{115}$$

Notice that the main difference between our estimation and the value used in the literature is the energy limit for which the primary spectrum is valid.

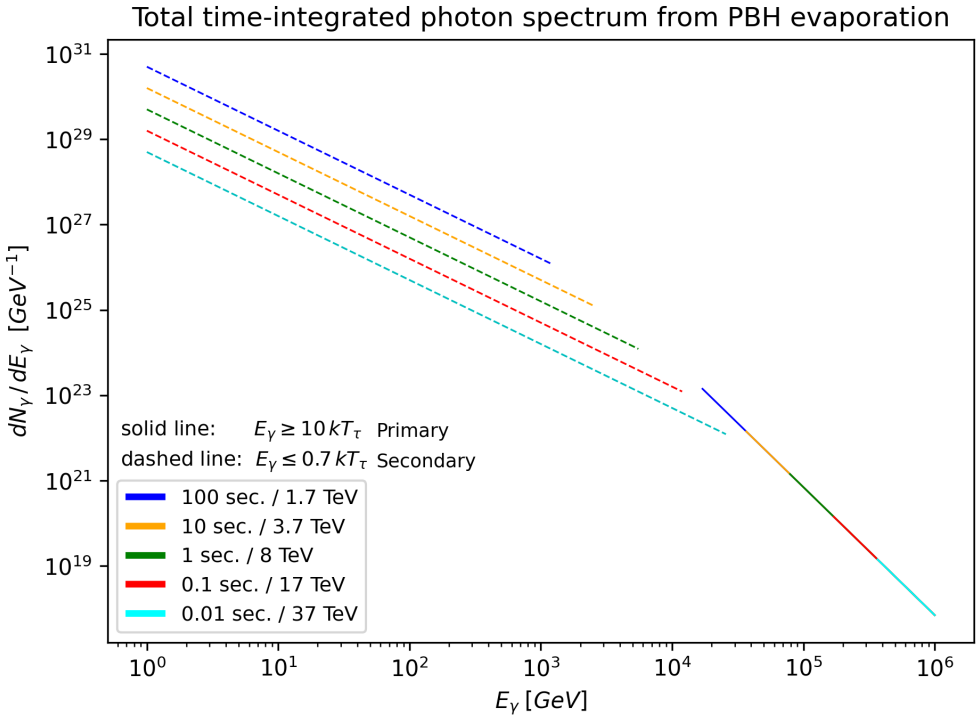

Figure 15: Total time-integrated photon spectrum from a BH evaporation, for different BH lifetimes in the last 100 seconds before full BH evaporation.

4 BlackHawk simulations

The essential part of our work is to understand and to identify the photon signal from a PBH evaporation. To achieve this, we calculated the photon spectrum treating the phenomenon as a blackbody emission and using Hawking's emission formula (see Section 1.2). In Hawking's theory, we must deal with greybody factors $\Gamma_s(x)$, that can only be obtained numerically. However, for a Schwarzschild BH, and assuming that emitted particles are relativistic (massless), we can use the approximations for $\Gamma_s(x)$ when $E \ll kT$ (low energy limit) for each spin species (Equation (62)), and $E \gg kT$ (high energy limit) for all species (Equation (63)), where E is the emitted particle energy. In the high energy limit, the energies of the emitted particles are much higher than the BH temperature, such that the particle wavelengths are much smaller than the BH radius. In this limit (also called the geometrical optics limit), the spectrum is dominated by particles that are directly emitted by the BH (primary spectrum). Indeed, this primary radiation reaches the black body radiation except for a 27/4 factor as we have discussed in Section 1.3. For the secondary spectrum, we assumed that the main source of photons is the neutral pion decay through the process $\pi^0 \to \gamma\gamma$. Given the complexity of the quark hadronization into pions, we have been forced to do crude approximations to calculate the neutral pion production. To test our calculations, we shall use `BlackHawk v2.0` [2, 3], which is a public program to simulate spectra due to Hawking's radiation from a distribution of BHs. This program allows us to simulate the spectra using numerical calculations for the greybody factors $\Gamma_s(x)$. Furthermore, we can estimate the secondary spectra due to the quark hadronization and the respective decay modes, using codes of hadronic physics programs such as `PYTHIA` and `HERWIG` [5, 19] that are incorporated in `BlackHawk`.

The instructions for the use of `BlackHawk` are well documented in its manual, which is available in its website [2, 3]. Briefly, the code runs two programs called `BlackHawk_inst` and `BlackHawk_tot` with parameter settings given in a `.txt` file, called `parameters`. The first routine gives the instantaneous spectrum for a mass distribution of BHs, and the second one gives the same quantity for each time interval (customized previously by the user) until almost full BH evaporation (the physics of the last instants close to Planck time is not known). Both routines calculate the primary and secondary spectrum for each species.

The output of `BlackHawk` is the spectral emission rate per comoving volume unit of species i defined as

$$\frac{d\dot{n}_i}{dE} = \int_{M_{min}}^{M_{max}} dM \, \frac{d\dot{N}_i}{dE} \frac{dn}{dM} \quad [\mathrm{GeV}^{-1}\mathrm{s}^{-1}\mathrm{cm}^{-3}], \tag{116}$$

where $d\dot{N}_i/dE$ is defined in Equation (29). Here, n is the total number of BHs per comoving unit volume (hereafter the BH number density). The comoving volume is defined as the volume for which a number density fixed to the Hubble flow, remains constant with redshift.

The quantity dn/dM is the mass distribution given the BH masses. Then, n can be written as a function of the mass distribution as

$$n = \int_{M_{min}}^{M_{max}} dM \, \frac{dn}{dM} \quad , \quad M_{\rm min} < M < M_{\rm max}. \tag{117}$$

The mass density (total BH masses per comoving unit volume) is

$$\rho = \int_{M_{min}}^{M_{max}} dM \, M \frac{dn}{dM} \quad , \quad M_{\rm min} < M < M_{\rm max}. \tag{118}$$

In this work we are interested in isolated BHs. Therefore, for a single BH of mass M_{BH}, the number of BHs in the comoving volume interval $[V, V + dV]$ is

$$dn = A \, \delta(M - M_{BH}) \, dM \tag{119}$$

where A has units of cm^{-3}. After inserting dn in Equation (116) we notice that output of `BlackHawk` is the spectral emission rate of species i per comoving unit volume

$$\frac{d\dot{n}_i}{dE_i} = A \frac{d\dot{N}_i}{dE_i}, \tag{120}$$

but for a single BH per comoving cm^3, $A = 1$ cm^{-3}. In order to simulate the primary and secondary photon spectrum with `BlackHawk`, we chose different PBH lifetimes in the range of 5 years to 0.01 seconds. These PBHs are shown in Table 1 with their respective temperatures and masses. Each simulation considers a single PBH. To calculate the corresponding lifetime τ due to the PBH mass, we have used the approximation of Equation (57). The lifetimes were calculated using the $\alpha(M_0)$ values found in Ref. [21] (see Figure 3). For PBHs with $kT < 100$ GeV we used $\alpha(M_0) \approx 7.0 \times 10^{26}$ g^3 s^{-1}, while for $kT > 100$ GeV we used the asymptotic value $\alpha_{SM}(M_0) = 8.0 \times 10^{26}$ g^3 s^{-1}.

Primordial black holes simulated on `BlackHawk`		
τ	M [g]	kT_τ
5 years	7.0×10^{11}	15 GeV
1 year	4.0×10^{11}	26 GeV
3 months	2.5×10^{11}	42 GeV
1 week	1.0×10^{11}	106 GeV
1 day	5.9×10^{10}	179 GeV
6 hours	3.7×10^{10}	286 GeV
30 min.	1.6×10^{10}	660 GeV
100 sec.	6.2×10^{9}	1.7 TeV
10 sec.	2.9×10^{9}	3.7 TeV
1 sec.	1.3×10^{9}	8 TeV
0.1 sec.	6.2×10^{8}	17 TeV
0.01 sec.	2.9×10^{8}	37 TeV

Table 1: Lifetime, mass and temperature of PBHs chosen to simulate the primary and secondary spectrum with `BlackHawk`.

4.1 Primary spectrum

The simulations of the primary photon spectrum are compared with the spectral emission rate of primary photons that we obtained using Hawking's emission formula with the approximation of the greybody factors $\Gamma_s(x)$ in the high energy limit for all species (see Section 1.3). This is

$$\begin{aligned}\left(\frac{d\dot{N}_\gamma}{dE}\right)^{(\mathrm{H})} &= \frac{2}{h}\frac{\Gamma^{(h)}(E/kT)}{e^{E/kT}-1} \\ &= \frac{27}{32\pi^2 h}\frac{(E/kT)^2}{e^{E/kT}-1} \quad , \quad E \gg kT,\end{aligned} \tag{121}$$

where the H superscript stands for Hawking's approximation. Additionally, we compare the simulations with the primary photon spectrum obtained with the black body approximation (BB), which according to the calculations in Section 1.3 it is related to Hawking's approximation as

$$\left(\frac{d\dot{N}_\gamma}{dE}\right)^{(\mathrm{H})} = \frac{27}{4}\left(\frac{d\dot{N}_\gamma}{dE}\right)^{(\mathrm{BB})} \quad , \quad E \gg kT. \tag{122}$$

Figures 16 to 18 show the simulations, Hawking's approximation, and the black body approximation of the primary photon spectra for PBHs of Table 1.

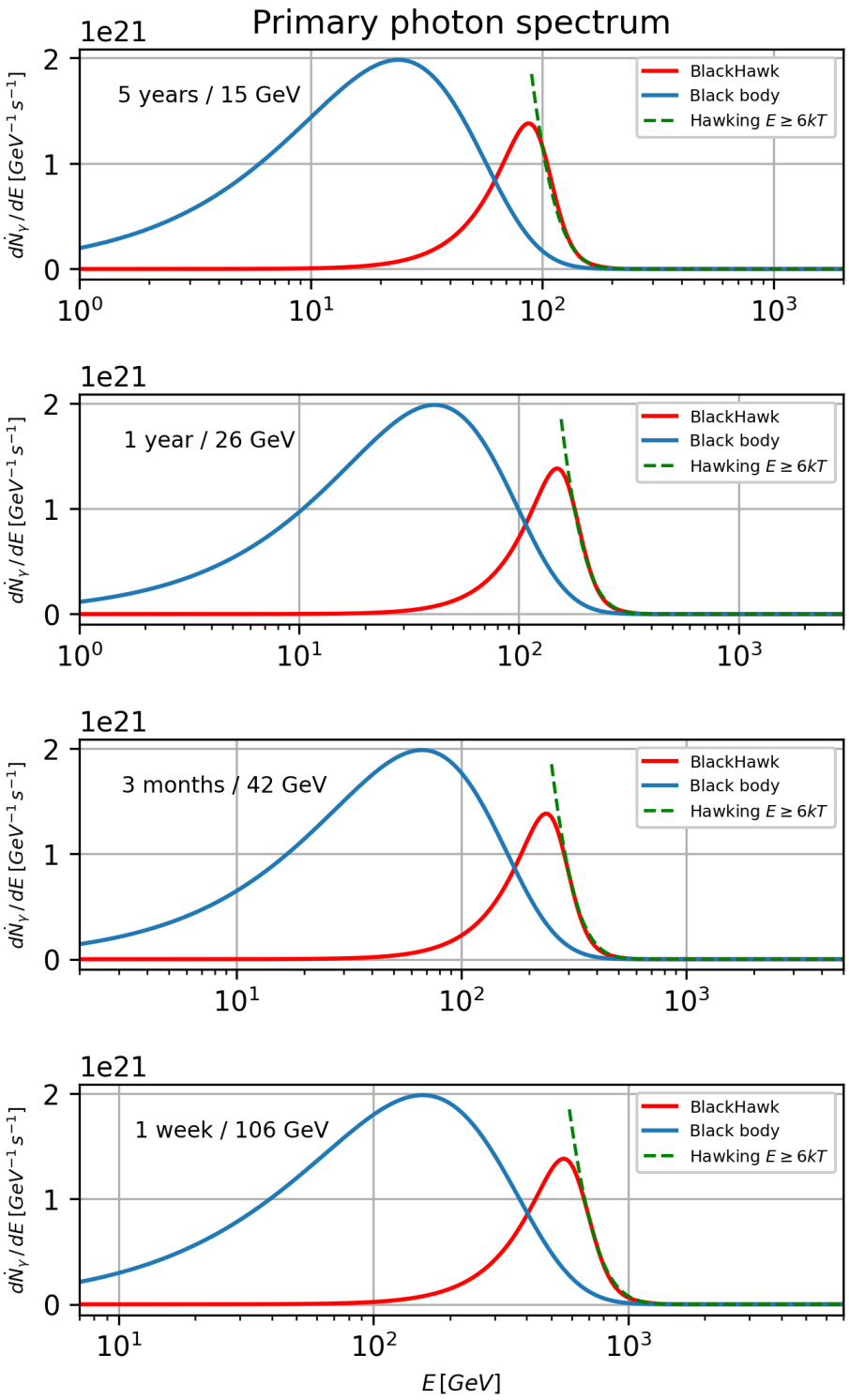

Figure 16: Primary photon spectrum of a PBH evaporation of lifetimes $\tau = 5$ years, 1 year, 3 months and 1 week, obtained with simulations in `BlackHawk`, Hawking's approximation in the high energy limit (for $E \geq 6kT$), and the black body approximation.

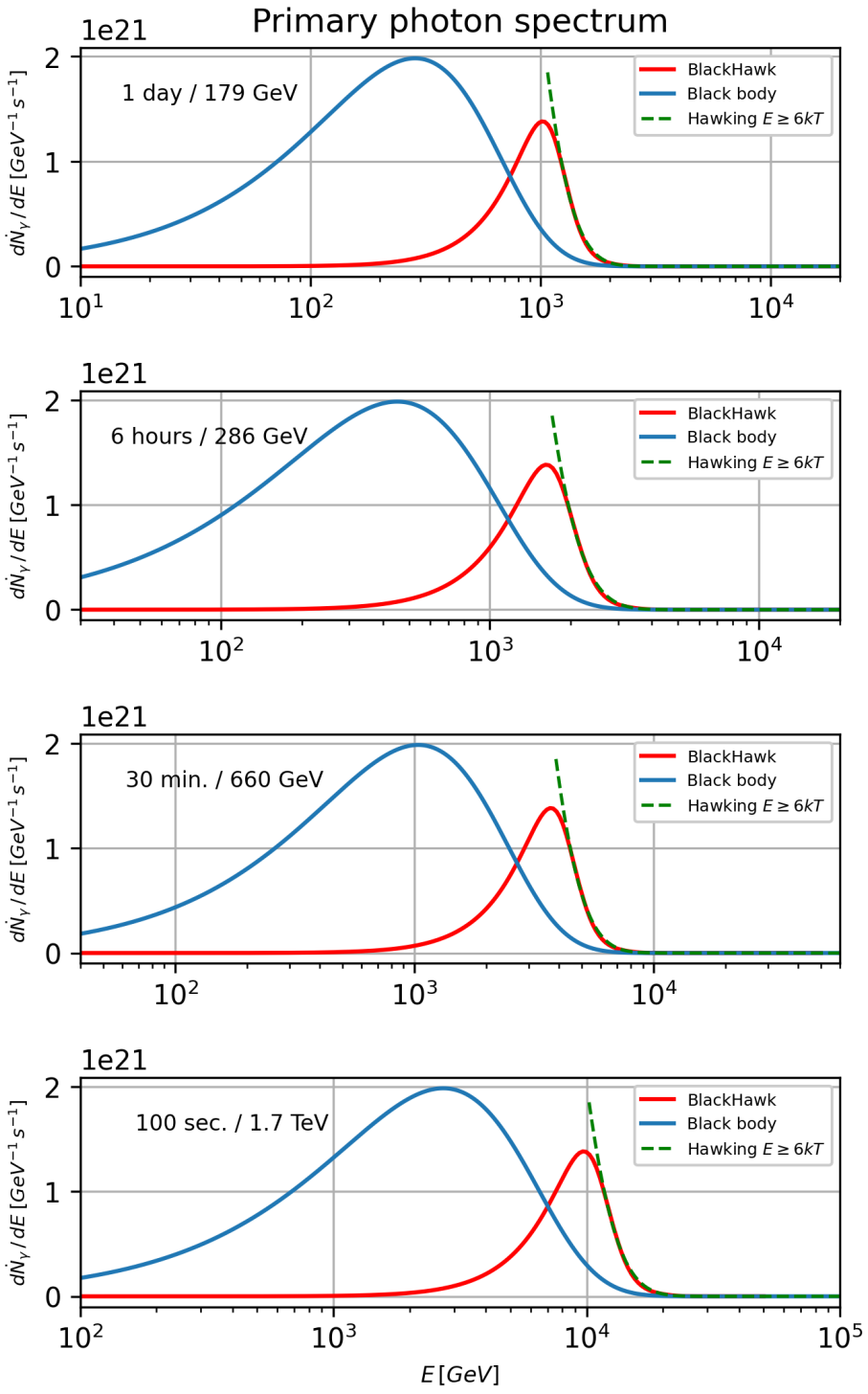

Figure 17: Primary photon spectrum of a PBH evaporation of lifetimes $\tau = 1$ day, 6 hours, 30 minutes, 100 seconds, obtained with simulations in `BlackHawk`, Hawking's approximation in the high energy limit (for $E \geq 6kT$), and the black body approximation.

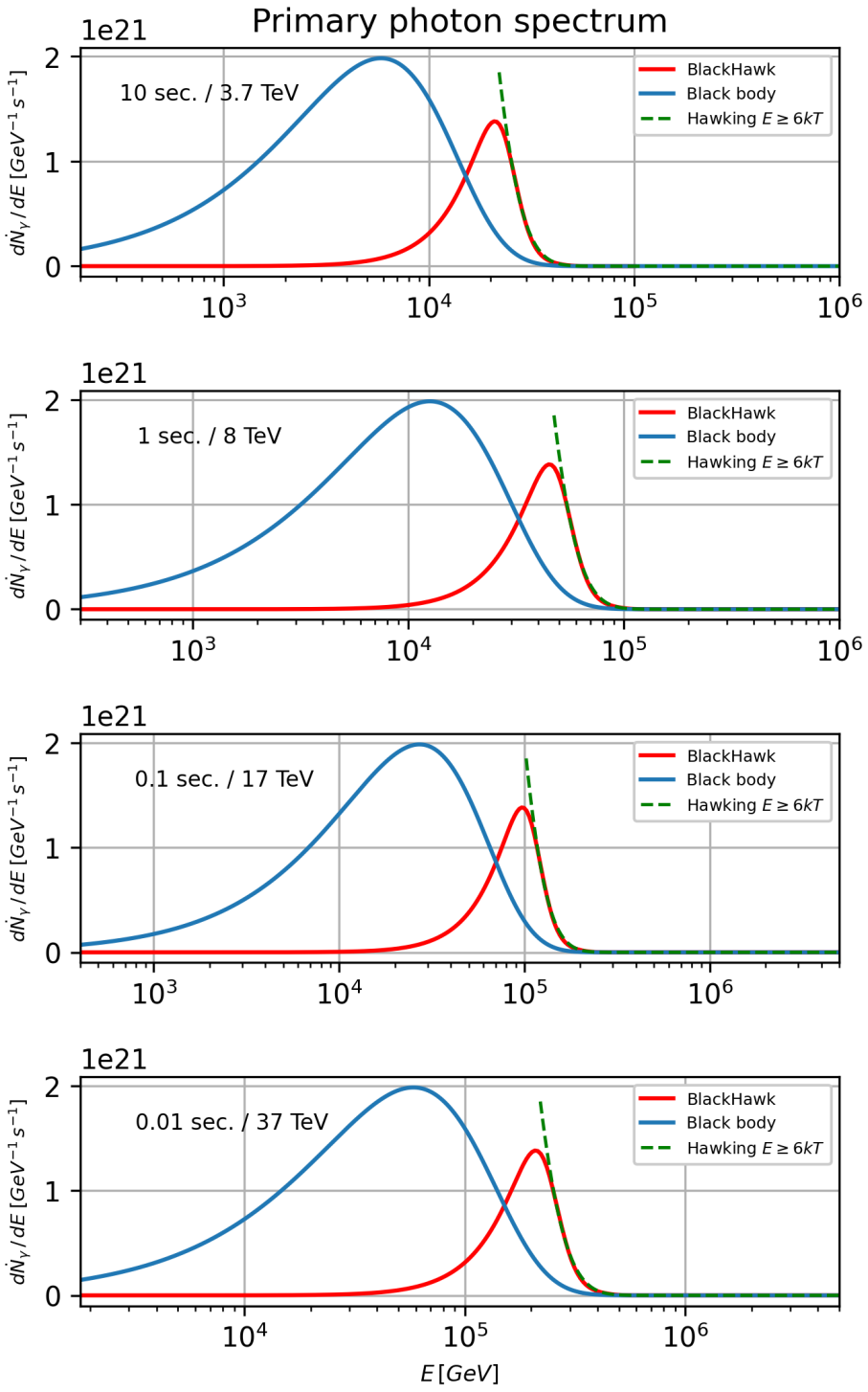

Figure 18: Primary photon spectrum of a PBH evaporation of lifetimes $\tau = 10$, 1, 0.1 and 0.01 seconds, obtained with simulations in `BlackHawk`, Hawking's approximation in the high energy limit (for $E \geq 6kT$), and the black body approximation.

The maximum of the spectral fluxes (peak heights) and the energy at the peak, are summarized in Table 2, for spectra obtained with simulations in `BlackHawk`, and with the black body approximation.

τ	`BlackHawk`		black body	
	Peak $\mathrm{GeV}^{-1}\mathrm{s}^{-1}$	E_{peak}	Peak $\mathrm{GeV}^{-1}\mathrm{s}^{-1}$	E_{peak}
5 years	1.4×10^{21}	87 GeV	2.0×10^{21}	25 GeV
1 year	1.4×10^{21}	148 GeV	2.0×10^{21}	42 GeV
3 months	1.4×10^{21}	236 GeV	2.0×10^{21}	67 GeV
1 week	1.4×10^{21}	554 GeV	2.0×10^{21}	157 GeV
1 day	1.4×10^{21}	1.0 TeV	2.0×10^{21}	286 GeV
6 hours	1.4×10^{21}	1.6 TeV	2.0×10^{21}	454 GeV
30 min.	1.4×10^{21}	3.7 TeV	2.0×10^{21}	1.0 TeV
100 sec.	1.4×10^{21}	9.7 TeV	2.0×10^{21}	2.8 TeV
10 sec.	1.4×10^{21}	20 TeV	2.0×10^{21}	6.0 TeV
1 sec.	1.4×10^{21}	45 TeV	2.0×10^{21}	13 TeV
0.1 sec.	1.4×10^{21}	97 TeV	2.0×10^{21}	27 TeV
0.01 sec.	1.4×10^{21}	208 TeV	2.0×10^{21}	59 TeV

Table 2: Maximum of the spectral fluxes and their respective peak energies of primary photon spectra obtained with simulations in `BlackHawk` and the black body approximation.

Spectra shown in Figures 16 to 18 plus the data summarized in Table 2 show us the following interesting results:

- The maximum of the simulated spectral fluxes are shifted to higher energies compared to the spectra of a black body.
- The photon spectrum obtained by Hawking's approximation in the high energy limit ($E \gg kT$), reproduces correctly the spectrum obtained with `BlackHawk` for $E \gtrsim 7\,kT$.

These results clearly show that Hawking's radiation spectrum is not the spectrum of a black body (Planck), but is shifted to higher energies. This can be understood because a BH is a very small emitter in size: $r_s \ll hc/kT_{BH}$. We will analyze this in more detail in Section 4.4.

Other interesting primary spectra are those of electrons and neutrinos, and when the PBH reaches temperatures $kT \gtrsim \Lambda_{QCD}$, the spectrum of quarks. The maximum of the spectral flux of each one of them is related to its statistics (Fermi-Dirac or Bose Einstein) and its degrees of freedom. These spectra are shown in Figure 19 for a PBH of lifetime 100 seconds.

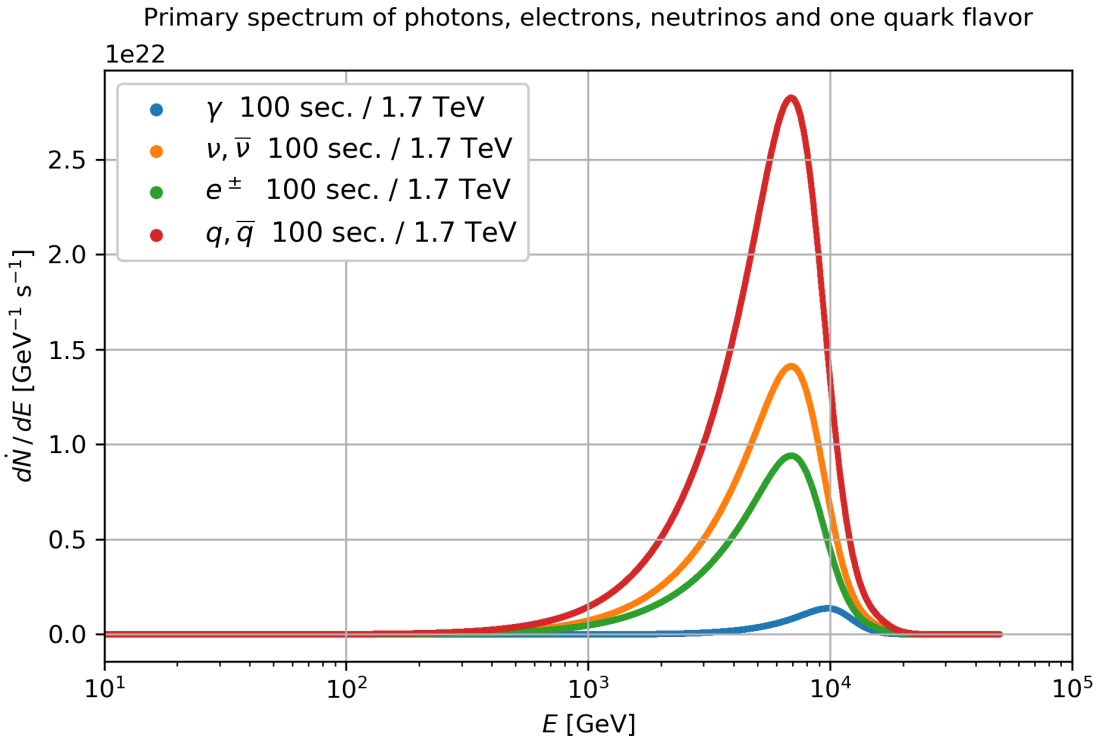

Figure 19: Electron, (Dirac) neutrino and one quark flavor primary spectrum radiated by a PBH of $\tau = 100$ seconds, obtained with simulations in `BlackHawk`. For this BH temperature, all emitted particles can be considered as massless particles.

Notice that, given to its larger number of degrees of freedom, electron, (Dirac) neutrino, and one quark flavor spectral fluxes are higher than the photon spectrum. In addition, according to Figure 19 the energy peak of photon spectrum is about $E_\gamma \approx 10$ TeV $\approx 6\,kT$, while the energy peak for electrons, neutrinos and on flavor quarks, i.e, fermions is about $E_f \approx 7$ TeV $\approx 4\,kT$.

4.2 Secondary spectrum

In the previous chapter, we considered the secondary photon spectrum obtained from $\pi^0 \to \gamma\gamma$ decay. Nevertheless, given the complexity of quark hadronization, we made rough assumptions that ended in an overestimation of pion production. This was corrected taking the leading terms of the spectral emission rate and the time-integrated spectrum (see Section 3.5). Using the program `BlackHawk_inst` we can obtain the secondary spectra for γ, ν, e^-, p^+. These stable particles are expected to be produced mainly by the decay processes of: neutrons and mesons (π, K, B, D, etc.), massive bosons $H^0, W^\pm, Z^0$, and unstable leptons (muons, tauons). Figures (20) and (21) show the proton spectrum and the secondary photon spectrum respectively.

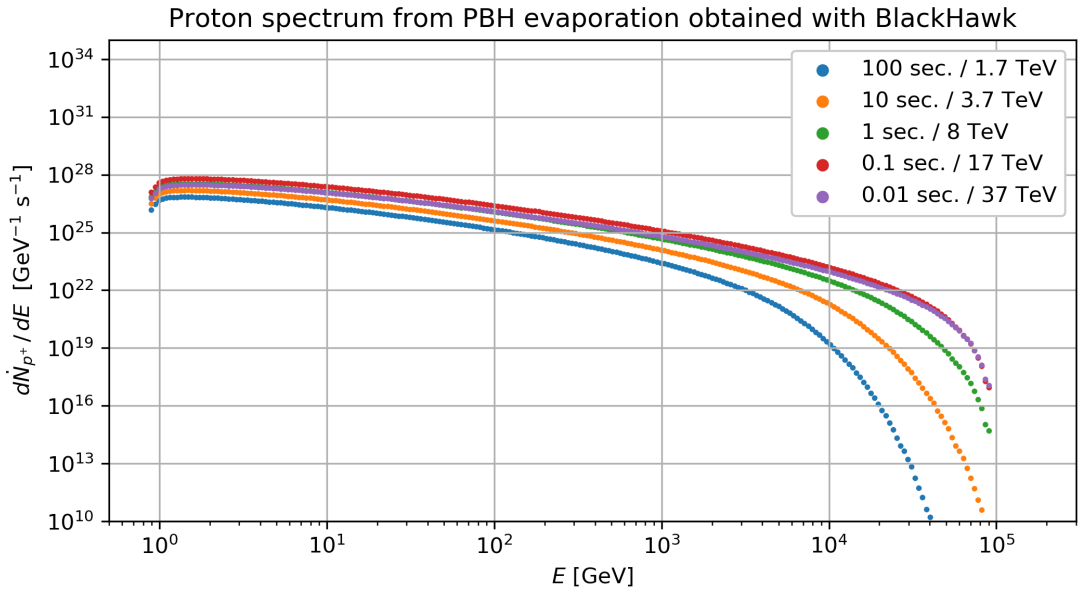

Figure 20: Proton spectrum from the evaporation of a PBH with lifetimes of $\tau = 100$, 10, 1, 0.1 and 0.01 seconds, obtained with simulations in `BlackHawk`.

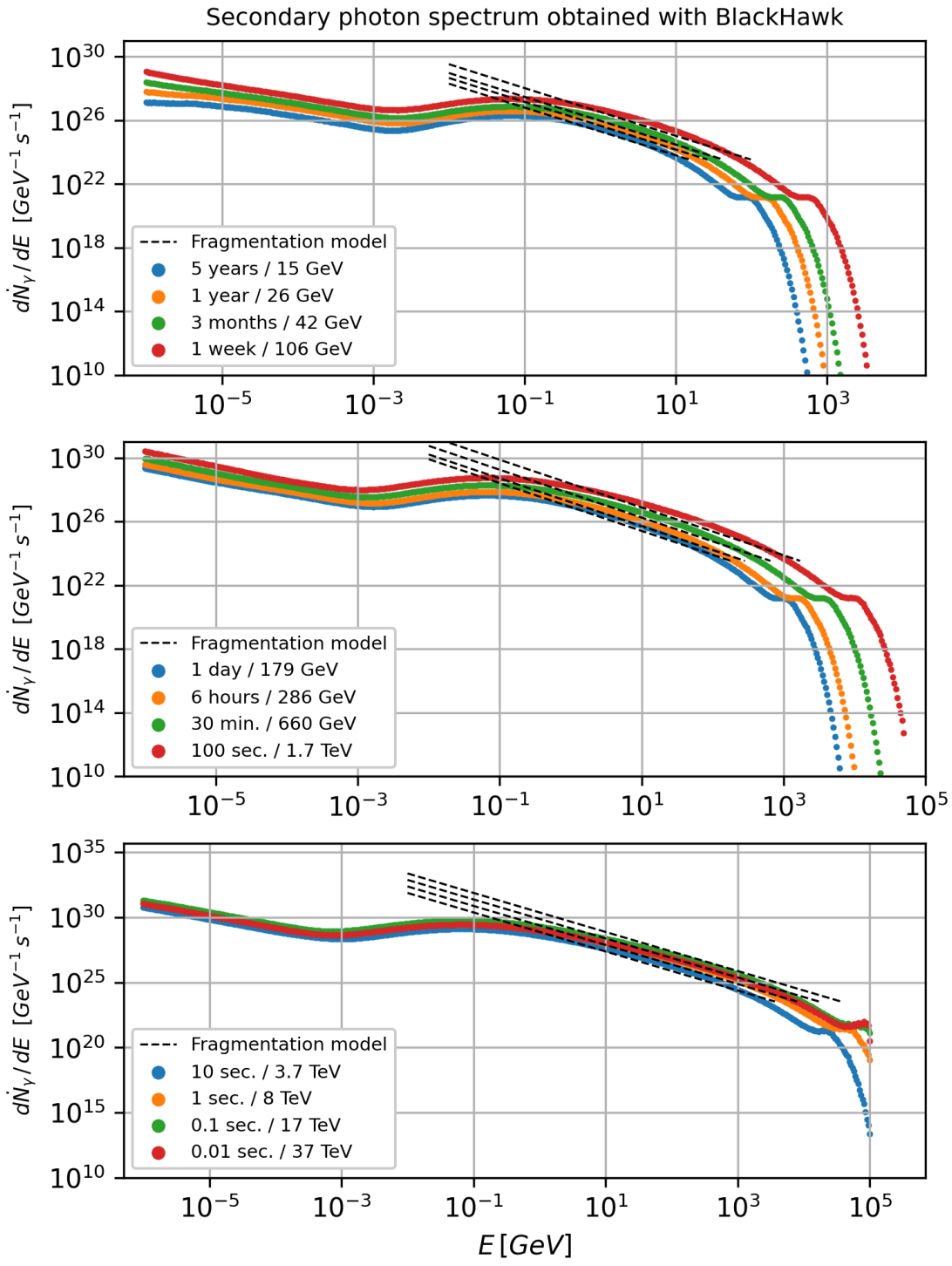

Figure 21: Secondary photon spectrum obtained with `BlackHawk` for the PBHs considered in Table 1. The dashed lines show the spectrum we predicted after corrected the π^0 overestimation (see Equation (111)).

4.3 Time-integrated spectrum

The program `BlackHawk_tot` calculates the spectrum at different times. In other words, lifetime τ is splitted on equal small intervals $dt_n = t_n - t_{n-1}$ such that spectral emission is evaluated at each time step t_n (fixed by `BlackHawk`). This allows us to do a discrete time-integration along a determined time interval. In order to compare our calculations of time-integrated spectra for primary and secondary photons (Equations (76) and (109) summarized in Equation (114)), we can obtain the time-integrated spectrum along the lifetime using:

$$\begin{gathered}\tau = t_1 + t_2 + \cdots + t_n \ , \ dt = t_n - t_{n-1} \\ \frac{dN_i}{dE_i} \approx \left.\frac{d\dot{N}_i}{dE_i}\right|_{t_1} dt_1 + \left.\frac{d\dot{N}_i}{dE_i}\right|_{t_2} dt_2 + \cdots\end{gathered} \tag{123}$$

It is important to remark that to run `BlackHawk_tot`, the input parameters need a finite BH mass remnant (mass leftover at the last instant before reaching the Planck mass), and therefore, the simulations cannot reach the final burst instant. However, the finite mass remnant can be very small, close to the Planck mass ($m_{Pl} \sim 10^{-5}$ g), which means lifetimes near to $t_{\rm Pl} \sim 10^{-44}$ s. For any BH with mass above $m_{\rm Pl}$ and times larger that $t_{\rm Pl}$, `BlackHawk` will compute the emission correctly. We set the BH mass relic equal to 10^{-4} g ($\tau \sim 10^{-40}$ s) indeed. The time-integrated spectra for primary and secondary photons of PBHs of Table 1 are shown in Figure 22.

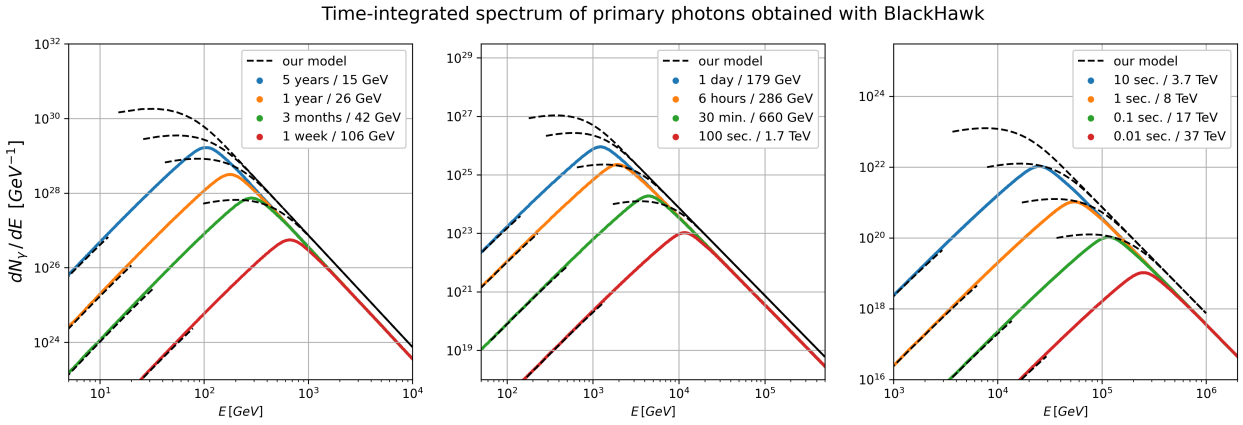

Figure 22: Time-integrated spectrum of primary photons obtained with `BlackHawk`. The dashed lines are the analytical approximation that we found using the Method of Brackets (Figure 8). Notice that both energy limits $E_\gamma \gg kT_\tau$ and $E_\gamma \ll kT_\tau$, are plotted.

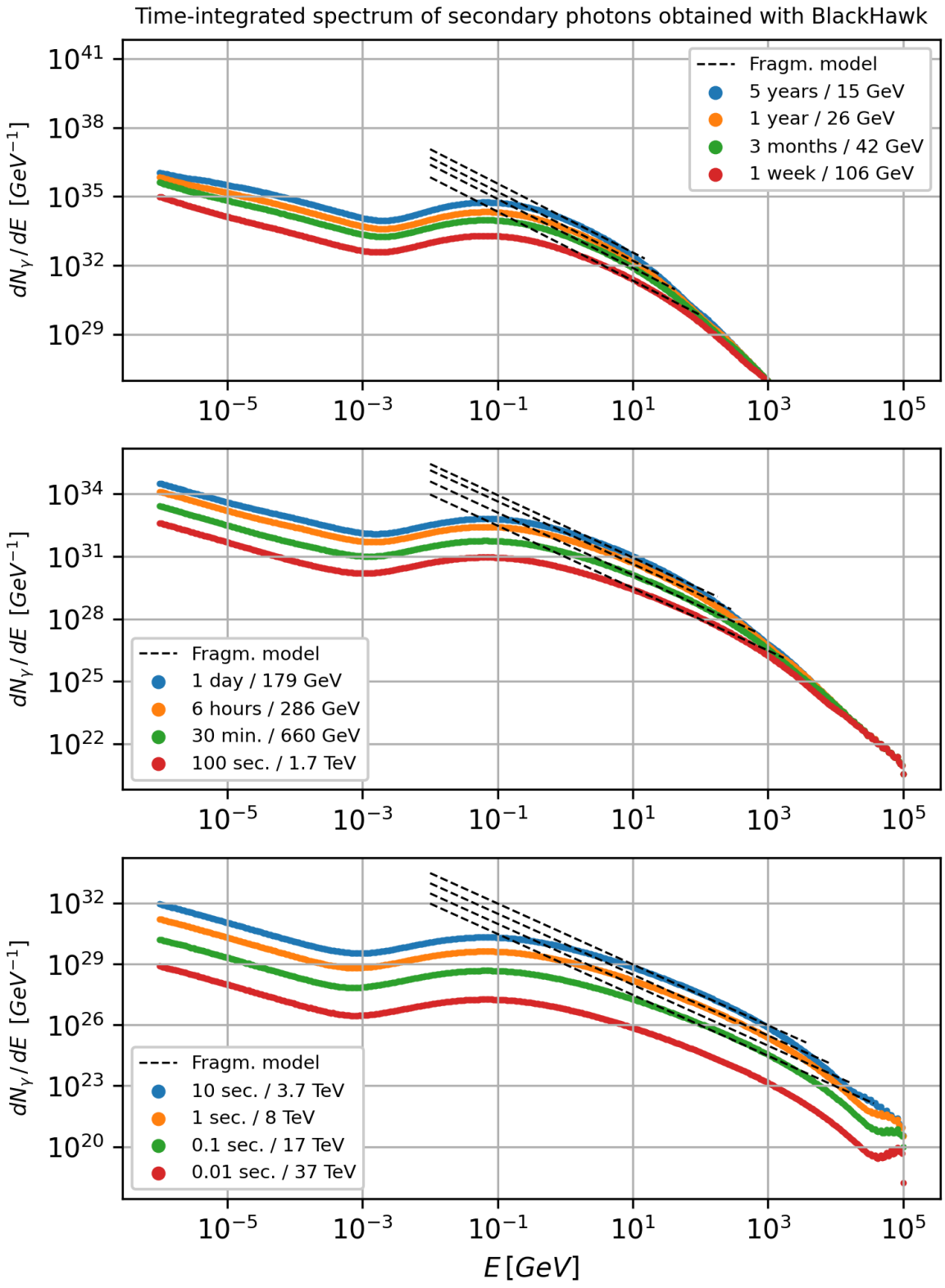

Figure 23: Time-integrated spectrum of secondary photons obtained with `BlackHawk`. The dashed lines correspond the fragmentation model that we used for our estimation (Equation (114)).

4.4 Small emitter

An interesting result that can be obtained analyzing the spectra simulated by `BlackHawk` is the understanding of the absorption coefficient $\Gamma_s(M, E)$, also called greybody factor. This function suppresses the emission of particles with wavelengths $\overline{\lambda} \sim hc/kT$. These wavelengths correspond to the typical emitted particles of a black body spectrum (particles with energies similar to the maximum spectrum energy). We can show that $\overline{\lambda}$ is always much larger than the BH radius, so a BH is a poor radiator of photons with $\overline{\lambda} \sim hc/kT$. From Equations (1) and (2), the BH temperature can be written in terms of the BH radius as:

$$kT = \frac{\hbar c}{4\pi r_s}. \tag{124}$$

Using the change of variable $x = E/kT$ and Equation (124), we can write the energy of the most typical particles $\overline{E}$ as:

$$\begin{aligned} \overline{E} &= x\, kT \\ &= \frac{\hbar c}{4\pi r_s} x. \end{aligned} \tag{125}$$

Using $\overline{E} = hc/\overline{\lambda}$ in Equation (125) we obtain

$$\frac{\overline{\lambda}}{r_s} = \frac{8\pi^2}{x}. \tag{126}$$

Let us consider a black body of temperature T_{BH} (Equation (28)). This spectrum reaches the maximum emission at $x \sim 1$. Then,

$$\frac{\overline{\lambda}}{r_s} \sim 8\pi^2 \sim 80. \tag{127}$$

Therefore, a black hole is too small to emit the same spectrum as of a black body of temperature T_{BH}, because the most emitted photons are no longer in the geometrical optics limit. Indeed, photons with wavelengths much larger than the Schwarzschild radius could not be efficiently produced by particle-antiparticle pair creation near the event horizon.

As `BlackHawk` calculates correctly the values of the $\Gamma_s(x)$ factors for all x, the spectrum obtained with simulations is correct. The simulated photon spectrum reaches its maximum at $x \sim 6$ (see Figure 19). This fact agrees with the result found in Ref. [21].

Then, for a Hawking photon spectrum, the ratio of the most typical wavelengths to the BH radius is:

$$\frac{\overline{\lambda}}{r_s} \sim \frac{8\pi^2}{6} \sim 13. \tag{128}$$

The $\Gamma_s(x)$ factor suppresses the emission at lower energies, where the wavelengths of the most typicial particles of a Planckian thermal spectrum are much larger than the BH size. As a consequence, the Hawking spectrum shifts the emission to higher energies where the geometrical optics limit is also satisfied, as Figures 16 to 18 show.

4.5 Chapter discussion

The primary spectra obtained with `BlackHawk` simulations showed us that the Hawking's radiation spectrum is definitely not a Planck thermal spectrum (black body). The maximum of a BH spectral flux is shifted to higher energies, supressing the typical photon wavelengths of the black body spectrum which are much larger than the BH radius. Additionally, we observed that approximations made in section 3.5 (Equations (110) and (113)) to correct for the π^0 overestimation were such that the secondary photon spectra are similar to spectra produced by `BlackHawk` simulations, except for the bottom plot of Figure 23. We ignore the reason behind this dissimilarity. The spectra in Figure 22 show that the time-integrated spectrum of primary photons obtained with `BlackHawk` does not have dependence on the initial BH temperature kT_τ for photons with energies $E \gtrsim 10\,kT_\tau$ as we predicted. This confirms our correction to the primary spectrum parametrization commonly used in Refs [15, 17, 21]. Figure 24 shows the total time-integrated photon spectrum according to our prediction as well as that obtained with `BlackHawk`.

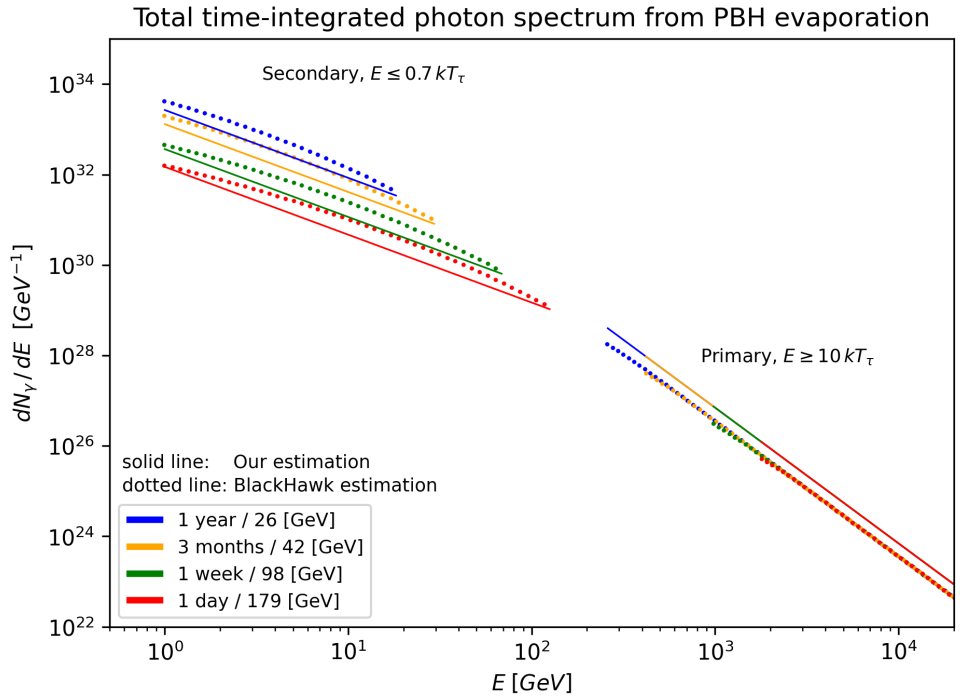

Figure 24: Total time-integrated photon spectrum according to our prediction (Equation (114)) as well as that obtained with `BlackHawk` simulations, for PBHs of lifetimes $\tau = 1$ year, 3 months, 1 week, 1 day .

Now that we have estimated the total photon spectrum, we shall study the eventual photon flux at the Earth's atmosphere. Then, we will run simulations of the electromagnetic cascades to obtain signatures of a PBH evaporation at a ground based detector level.

5 Flux on Earth

To count photons from a PBH evaporation that collide with the Earth's upper atmosphere, we shall assume that: (1) The medium between the PBH and Earth is transparent. We shall ignore other gamma ray sources such as gamma ray bursts (GRBs), supernova explosions, gamma ray background, BH jets; (2) we consider that the spectrum is due to a single PBH. We evaluate the emission of the PBH at the lifetimes of Table 1.

The photons (gamma rays) from a PBH evaporation can be detected using gamma ray space telescopes (such as Fermi-LAT) or ground based gamma ray observatories. The former captures gamma rays directly, while the latter reconstructs the electrons, positrons and photons cascade (the electromagnetic shower) produced by the interaction between the gamma ray and the atmosphere. This shower can be reconstructed observing the Cherenkov radiation pulse produced in the upper atmosphere by means of imaging air Cherenkov telescopes (such CTA gamma ray observatory), or by means of an array of particle detectors on the ground at sufficiently altitude. We shall assume that the gamma ray detection is through Water Cherenkov Detectors (WCDs). Among the gamma ray observatories with this technology are HAWC and LHAASO in the northern hemisphere, and SWGO (under design phase) in the southern hemisphere. The WCDs detection method consists in capturing the Cherenkov radiation produced in the water using photomultipliers located inside the tank. This radiation is produced by the shower particles that reach the ground. This detection method has the advantage to have a wide field of view (almost the whole visible sky) and observations with almost 100% of duty cicles (it observes all the time). Therefore, we shall assume a continuous observation time of at least 5 years.

Given that we solved the time-integrated photon spectrum, the signal of a PBH evaporation of a certain lifetime, is the number of photons within a certain energy interval, during a certain observation time interval. We must remark that we ignore the PBH lifetime, but we can search for the signature emission of a determined PBH lifetime fixing the energy interval and the observation time interval. In our case, we consider the PBH lifetimes shown in Table 1. For example, the signature emission of a PBH of lifetime $\tau = 5$ years, is the number of photons observed during 4 years within a energy interval $[E_1, E_2]$. This number of photons can be obtained as the difference between the time-integrated spectrum of a PBH of lifetime $\tau = 5$ years integrated in the energy interval $[E_1, E_2]$, and the time-integrated spectrum of a PBH of lifetime $\tau = 1$ year integrated in the energy interval $[E_1, E_2]$. Notice that if this difference is zero, there is no photon detection because the emission is due to a PBH with a lifetime $\tau < 1$ year.

This can be generalized for any PBH lifetime: the number of photons per km^2 detected during an observation time T, within the energy interval $[E_1, E_2]$ given a PBH evaporation

of lifetime τ, located at a distance d from Earth is:

$$N_\gamma^{(\tau)}(T) \approx 6\times 10^4 \left(\frac{d}{\text{pc}}\right)^{-2} \int_{E_1}^{E_2} dE \left[\left(\frac{dN_\gamma}{dE}\right)^{(\tau)} - \left(\frac{dN_\gamma}{dE}\right)^{(\tau')}\right] \quad \text{for} \quad T=\tau-\tau'>0, \tag{129}$$

where

$$\left(\frac{dN_\gamma}{dE}\right)^{(\tau)} = \int_0^\tau dt\, \frac{d\dot{N}_\gamma}{dE}, \tag{130}$$

is the time-integrated spectrum, that we obtained analytically (Equation (114)) and using simulations in `BlackHawk` (Section 4). Notice that $dN_\gamma^{(\tau)}/dE$ contains the primary and secondary photon spectrum.

Equation (129) can be integrated, either using our approximation for the total time-integrated spectra, or using the one obtained with `BlackHawk`. Despite our prediction has a good fit with simulated spectrum (see Figure 24), we shall use the total time-integrated spectrum from `BlackHawk` to integrate Equation (129) numerically. However, according to Figure 24 we need the spectrum in the energy interval $[0.7kT_\tau\,,\,10kT_\tau]$ to do the integration. As the dependence on the initial BH temperature is lost in the primary spectrum for photons with energies $E \gtrsim 10kT_\tau$, we shall assume that the secondary spectrum is valid for photons with energies $E \leq 10kT_\tau$. Figure 25 shows the numbers of photons per km^2, observed during fixed observation time intervals, within six energy intervals that cover low to high energy photons, for PBH of lifetimes shown in Table 1. We consider three distances for PBH locations.

Unlike other very high energy (VHE) gamma ray sources, such as GRBs and supernova explosions, the short duration of the VHE photon emission due to a PBH evaporation in the last 100 s, can be a PBH photon signature. Additionally, from plots with energy intervals $[10, 100]$ TeV and $[100, 500]$ TeV of Figure 25, we notice that emissions from a PBH located at 1 pc from Earth are undetectable, i.e, VHE gamma rays from a PBH evaporation can be detected locally ($d < 1$ pc), while GRBs can be detected at cosmological distances. Despite the number of photons decreases when the detection energy interval is increased, the higher energy intervals are sensitive to the last stages of PBH evaporation ($\tau < 30$ min).

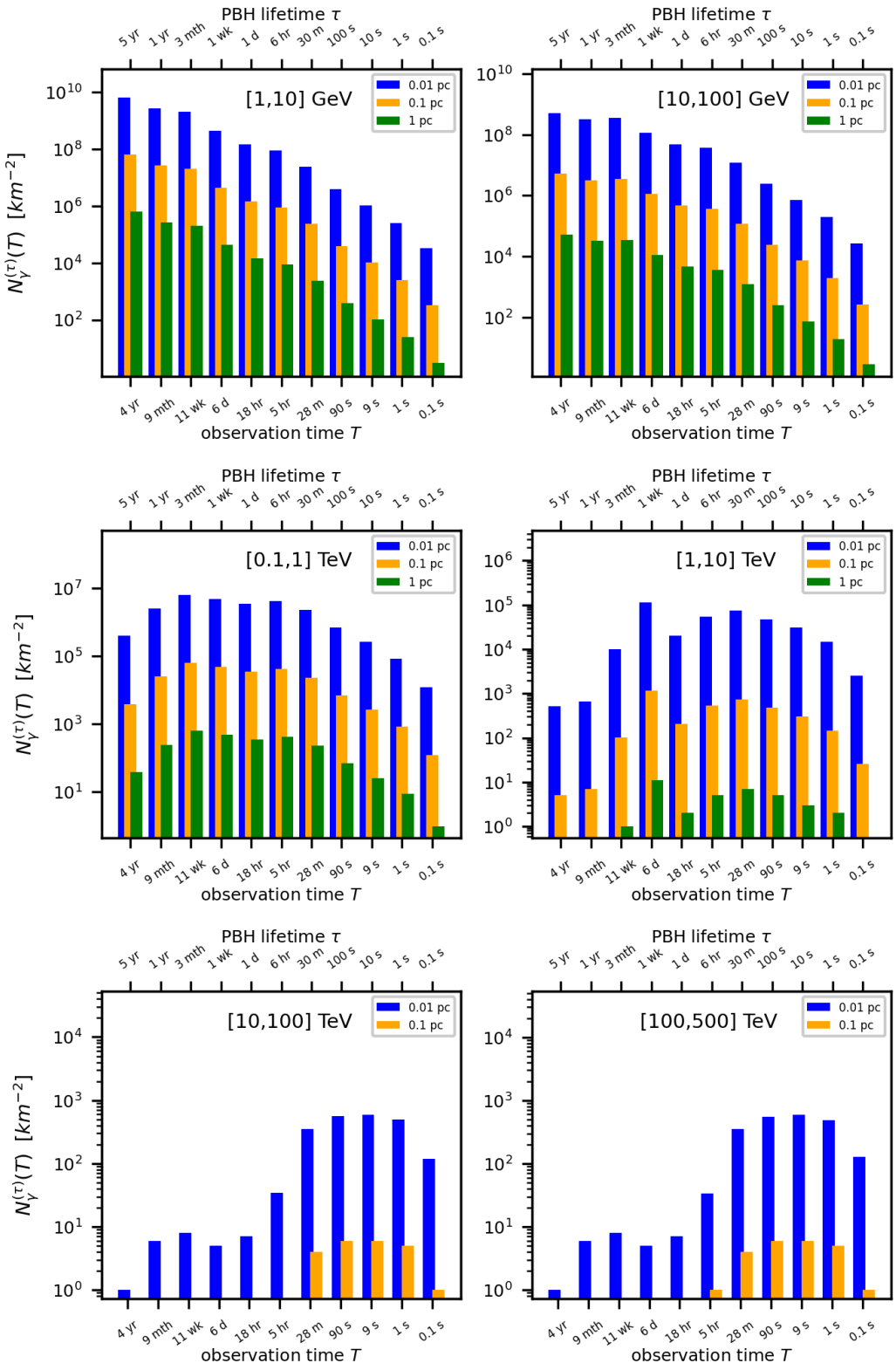

Figure 25: Number of photons per km^2 that collide with the atmosphere during different observation times. We chose these observation times to detect photon signals from PBH of lifetimes shown in Table 1. We consider six energy intervals, and three PBHs locations from Earth: 0.01, 0.1 and 1 pc.

6 Gamma ray detection

6.1 Electromagnetic shower

Now that we have an estimation on the number of photons that reach the Earth's atmosphere within a certain energy interval during a fixed observation time, we want to know the electromagnetic shower in the atmosphere produced by a photon of a given energy. In particular, a high energy photon (GeV energies) can produce a high energy electron-positron pair. The electrons and positron will lose energy by radiation due to the interaction with the nuclei in the atmosphere (Bremsstrahlung). The resulting photons (with less energy than the primary photon) will undergo pair production again or Compton scattering. This cascade will stop when the energy of the resulting photons is below a critical energy. As a result, a large amount of electrons, positrons and photons are produced. If a high energy electron ($E \gg mc^2$) is moving through the atmosphere along X coordinate, its energy E varies with the coordinate X according to:

$$\frac{dE}{dX} \approx -\frac{E}{X_0}, \tag{131}$$

where X_0 is a constant called radiation length, and it depends on the material. For example, X_0 for water is about 36 cm, and air about 300 m under 20 °C and 1 atm. This quantity is typically measured in g cm^{-2}. This form to measure the radiation length expresses the amount of matter that is passing per unit area. Integrating Equation (131) we find the average energy distribution at distance X which is:

$$E(X) = E_0\, e^{-X/X_0}. \tag{132}$$

One effective model that describes the electromagnetic shower is the Heitler model (late 1930s). In this approximation, it is assumed that each particle of the shower travels one radiation length and then is split into two particles with equal energy (Figure 26). Also, it is assumed that pair production and bremsstrahlung are the only processes that produce the shower. As a consequence, this model predicts roughly 2^n particles for n radiation lengths. As the energy is equally distributed on the total number of particles at each splitting step, we can write

$$E_n = \frac{E_0}{2^n}. \tag{133}$$

Using the fact that $X = n\, X_0$ and inserting in Equation (133) we obtain

$$X = X_0 \log_2\left(\frac{E_0}{E_n}\right). \tag{134}$$

When the rate of energy loss by radiation is equal to the rate of energy loss by ionization, there is no longer particle creation, and therefore, the shower development stops. This occurs when the energy reaches the critical value $E_n = E_c$, and the particle has reached the length for which shower has reached the maximum particle multiplicity X_{max} (for more details see Ref. [1]). This can be written as:

$$X_{max} = X_0 \log_2 \left(\frac{E_0}{E_c} \right). \tag{135}$$

Indeed, given that particle production has stopped, the maximum number of shower sub-particles can be obtained using Equation (133) such that

$$N_{max} = \frac{E_0}{E_c}. \tag{136}$$

To have an idea of the actual distance comparatively to a given X, we assume that the atmosphere is isothermal, so the amount of atmosphere matter per unit area, X (also called the atmospheric thickness), varies with height h measured in km, according to

$$X = 1030\, e^{-h/6.5} \quad \text{g cm}^{-2}. \tag{137}$$

The amount of matter per unit area contained in the atmosphere ($h = 0$) is 1030 g/cm^2, which is the total vertical atmospheric depth.

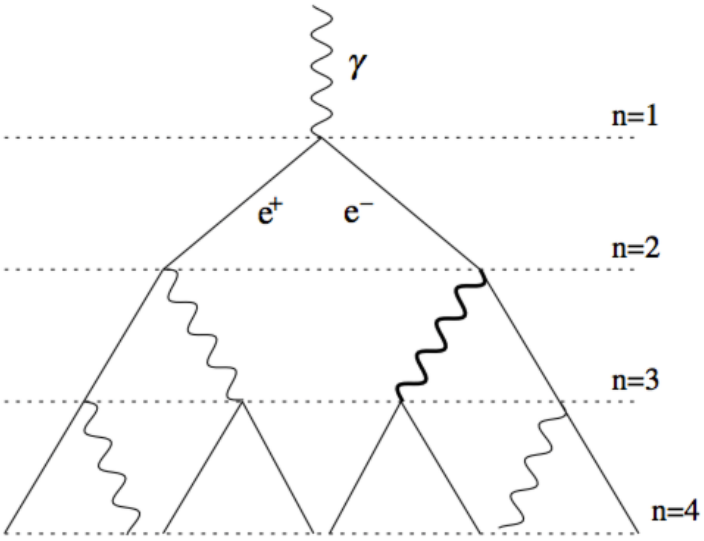

Figure 26: Heitler model representation.

6.2 `Corsika` simulations

We are interested in studying the basic features of the electromagnetic showers produced by photons (hereafter γ-rays) coming from a PBH evaporation. To achieve this, we shall use `Corsika` (version 7.7), a powerful program used to simulate extensive air showers produced by cosmic rays [14]. Briefly, this program is equipped with many routines that incorporates different models for shower development of hadrons, nuclei, neutrinos, and γ-rays. There are two models that describe electromagnetic showers. One model is based on simulations with Monte Carlo, called EGS4. The another, reconstructs the shower using the solutions of Nishimura-Kamata-Greisen equations, so it is called NKG. To run simulations of an electromagnetic shower due to a γ-ray, we must define an input card with physical and programming parameters. The main physical parameters that we need to fix are:

- The type of primary particle. For our case, we set photon.
- The energy range of the primary particle $[E_0^{min}, E_0^{max}]$. We fixed the energy of primary particle, instead of using an energy range.
- The azimuthal angle ϕ , and inclination angle θ measured between particle momentum and vertical coodinate Z.
- Earth's magnetic field at the event location. In this parameter we used a place near to ALMA Observatory, over 4700 m.a.s.l located at $(22.93^\circ\ \mathrm{S}, 67.68^\circ\ \mathrm{W})$. The values of the magnetic field for this location were calculated with IGRF model on the NOAA webpage [8].

According to the results of Section 5, we shall simulate the shower of three gamma rays in the low, medium and very high energy regime. Table 3 shows the energies and inclinations chosen for `Corsika` simulations.

γ-ray	E_0 TeV	(θ, ϕ) deg
γ_1	300	(8,0)
γ_2	12	(0,0)
γ_3	0.5	(0,0)

Table 3: γ-rays chosen for `Corsika` simulations.

All simulations were run with the following models:

- High energy hadronic interaction model: QGSJET II
- Low hadronic interaction model: URQMD
- Horizontal flat detector located at 4700 m.a.s.l.
- Electromagnetic model: EGS + NKG

Table 4 summarizes the main information extracted of each shower.

Gamma ray	Z_{first} km	X_{max} m.a.s.l	N_γ	N_{e^-}	N_{e^+}	$N_{\mu^\pm}$
γ_1	17	≈4000	$9{\times}10^5$	1×10^5	$9{\times}10^4$	179
γ_2	17	≈5000	$4{\times}10^4$	$5{\times}10^3$	$3{\times}10^3$	6
γ_3	17	≈7000	$9{\times}10^2$	93	52	0

Table 4: Parameters of electromagnetic shower of γ-rays shown in Table 3, simulated with `Corsika`.

In Table 4, $N_{\gamma,e,\mu}$ are the number of $\gamma, e^\pm$ and $\mu^\pm$ respectively counted at the detector level. The parameter Z_{first} is the height of the first interaction of the γ-ray with the upper atmosphere. The parameter X_{max} is the approximate height (measured from sea level) for which the γ-ray shower reaches its maximum multiplicity. We used Equation (137) to estimate this quantity in km. Notice that only the γ_2 and γ_3 showers reached their X_{max} before reaching the detector level. The shower signature printed at the ground depends on the number and type of subparticles, and their energy distribution at the detector level. Figures 27 to 29 show the spatial distribution of electromagnetic shower subparticles $(\gamma, e^\pm)$ at the detector level.

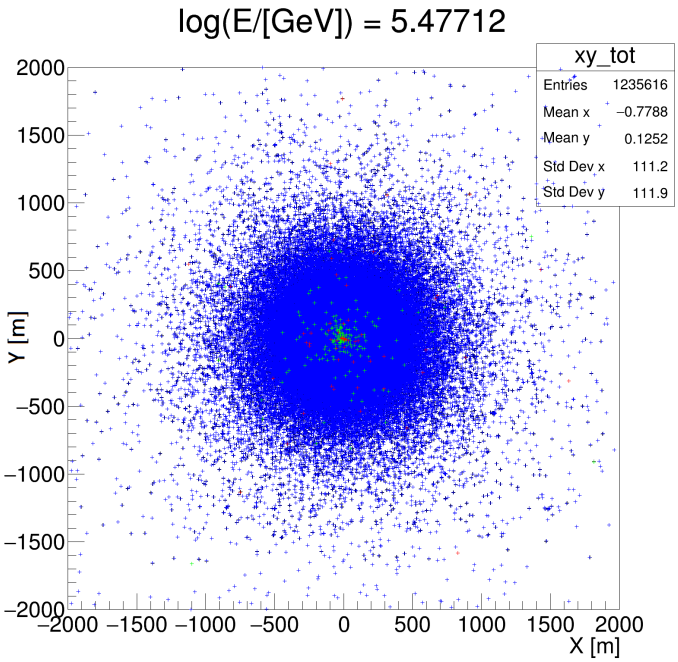

Figure 27: Footprint of an electromagnetic shower produced by a γ-ray of energy $E_0 = 300$ TeV, azimuthal angle $\phi = 0$, and inclination $\theta = 8$ degrees. In green (red) electrons (positrons). Note that although this gamma ray collided the atmosphere with an inclination, the development of the shower is symmetrical respect to the vertical axis.

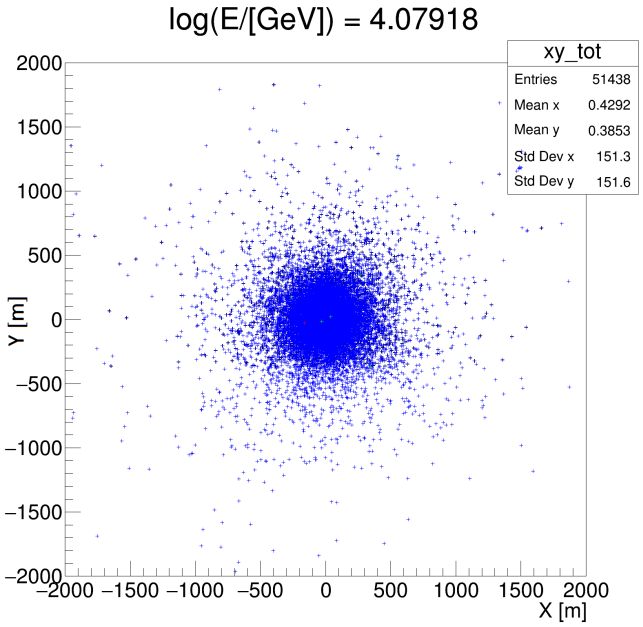

Figure 28: Footprint of an electromagnetic shower produced by a γ-ray of energy $E_0 = 12$ TeV and inclination $\theta = 0$ degrees.

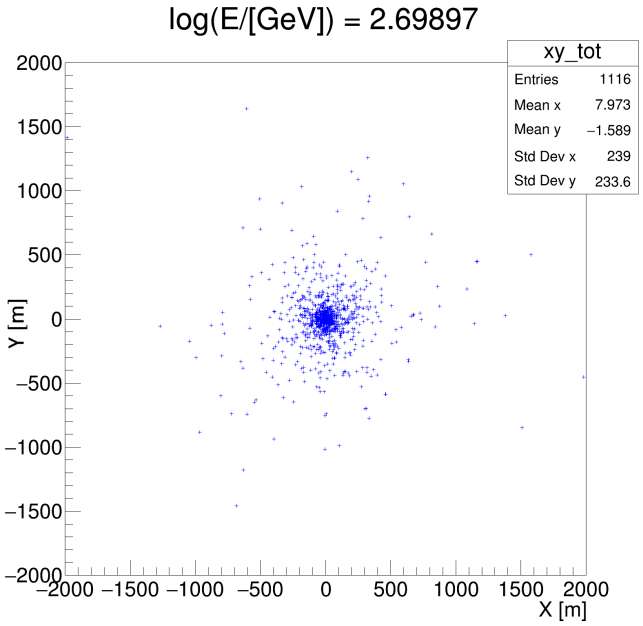

Figure 29: Footprint of an electromagnetic shower produced by a γ-ray of energy $E_0 = 500$ GeV and inclination $\theta = 0$ degrees.

Although γ_1 could not reach its X_{max}, its footprint is a dense shower of photons, electrons and positrons contained in a region of about 1 km^2. The footprint of γ_2 and γ_3 are regions of about 0.5 km^2 and 0.03 km^2, respectively.

Figure 30 shows the momentum (energy) distribution of the electromagnetic shower particles ($\gamma, e^{\pm}$) at the detector level. Figure 31 shows atmospheric development of the electromagnetic showers on the XZ plane of γ_1, γ_2, and γ_3.

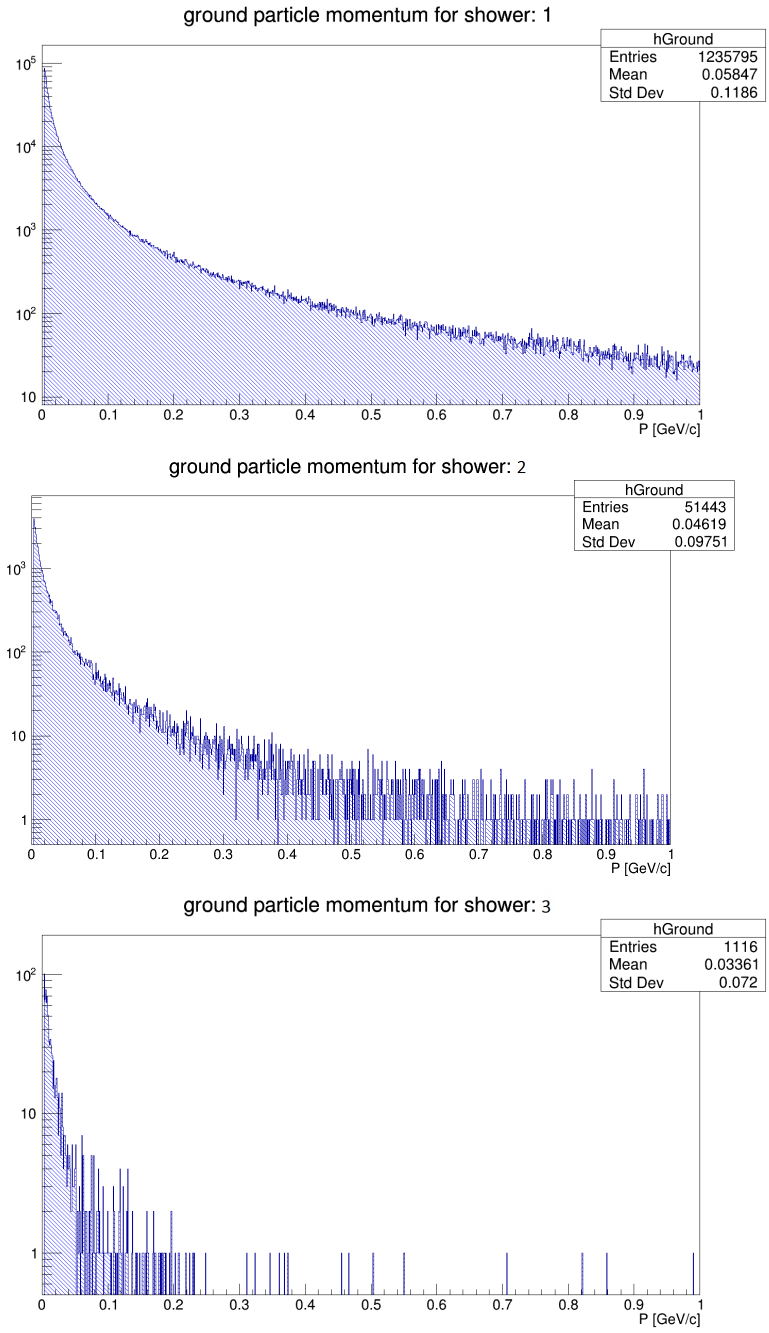

Figure 30: From top to bottom, momentum (energy) distribution of shower particles at the detector level of γ_1, γ_2 and γ_3. The number of entries for each plot are the total number of particles at detector level ($e^+ + e^- + \gamma$). Notice that for a γ-ray of $E_0 = 300$ TeV, a significant number of particles (mainly photons) reach the detector level with $E \sim 1$ GeV. For γ_2 and γ_3 this number is negligible.

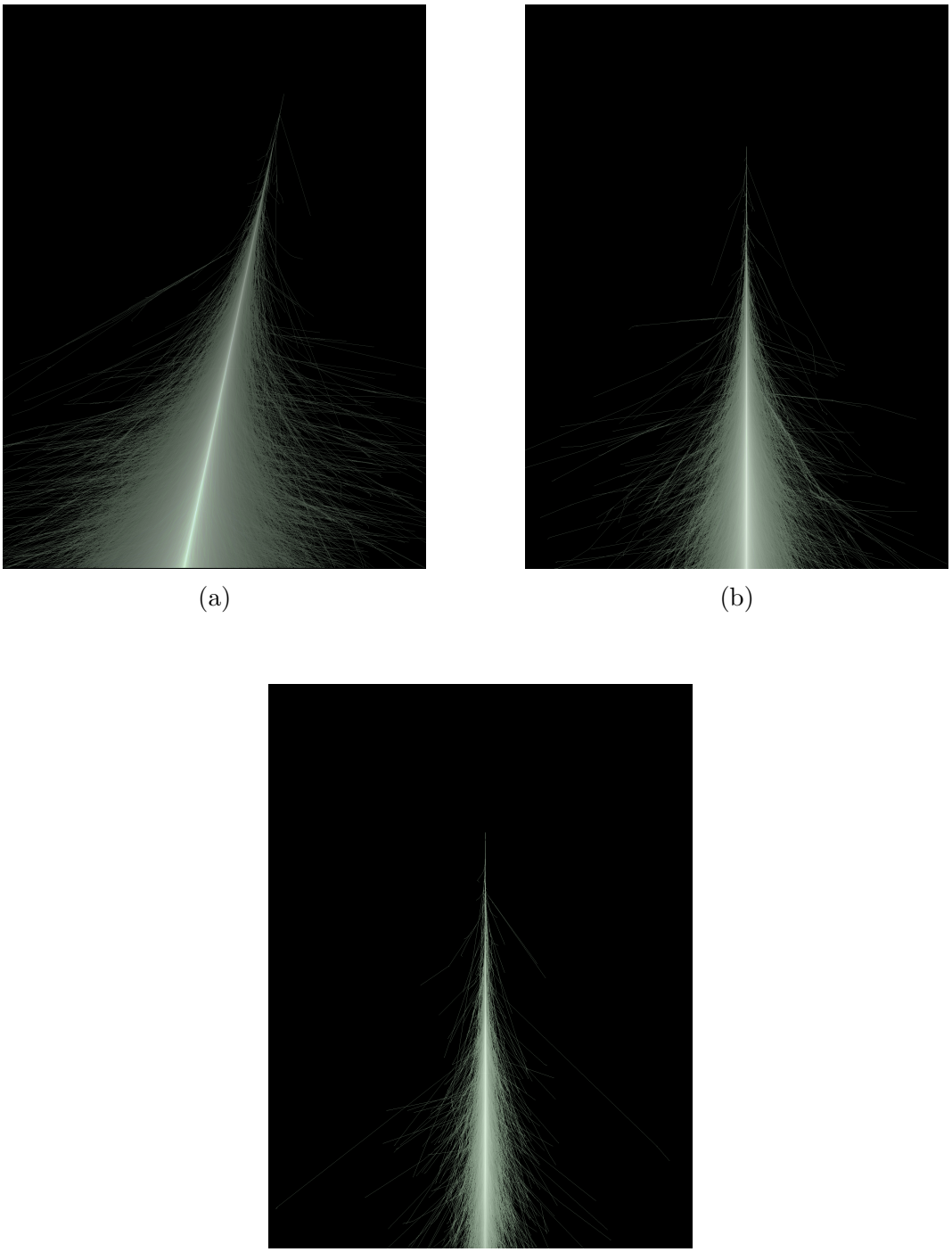

(a) (b)

(c)

Figure 31: Atmospheric development of the electromagnetic shower on the XZ plane for a γ-ray with energy: (a) $E_0 = 300$ TeV and direction $(\phi, \theta) = (0, 8)$ deg; (b) $E_0 = 12$ TeV and direction $(\phi, \theta) = (0, 0)$ deg; (c) $E_0 = 500$ GeV and direction $(\phi, \theta) = (0, 0)$ deg. Notice that unlike the shower (a), the showers (b) and (c) reached their X_{max}.

7 Discussion and Conclusions

The Hawking radiation spectrum is not a Planckian thermal spectrum. The BH evaporation is a phenomenon where the emitter size is too small to emit the spectrum of a black body with temperature T_{BH}. Instead, a BH spectrum is characterized by the absorption coefficient $\Gamma_s(x)$, also called greybody factor. This function is the probability that the emitted particle could escape to infinity under the gravitational field of the BH. The greybody factor depends on the BH mass, the energy and the spin of the particle species i, and must be calculated numerically to obtain the correct spectral emission rate of species i. Nevertheless, analytical approximations for $\Gamma_s(x)$ have been found in the limit $E \gg kT$ [16]. In this limit, the greybody factor converges to the geometrical optics limit for all spin species. For photons, this limit corresponds to the black body radiation. However, we noticed that the BH radiation spectrum exceeds the black body by a factor 27/4 at $E \gg kT$. This fact raises questions about the correctness of the asymptotic value of $\Gamma_s(x)$ in this energy limit. The disagreement between the BH radiation and the black body radiation demands to have a better understanding of the phenomenon on a theoretical basis. This is left for future work.

Using certain approximations ($\delta = 0$ in Equation (64)), and using the Method of Brackets to time-integrate the spectral emission rate along the BH lifetime, we found a new expression of the time-integrated spectrum of primary photons. This result corrects the value of the time-integrated primary spectrum used in Refs. [15, 17, 21]. Our result shows that the spectral emission of primary photons decreases as a function of the photon energy according to $dN_\gamma/dE \propto E^{-3}$, for photons with energies $E_\gamma \gtrsim 10\, kT_\tau$ (see Equation (76)). To estimate the secondary photon spectrum, we obtained the π emission doing crude assumptions about quark hadronization, that ended in an overestimation of the secondary photons because we considered all decays as hadronic, disregarding lepton emission. In addition, a term of the fragmentation function produced an increase of pion emission with energies $E_\pi \geq kT_\tau$. Using some approximations, and taking the leading term of the spectral emission, we reproduced similar values as those used in Refs. [15, 17, 21] (see Section 3.5). As a consequence, we found the total photon spectrum of a PBH evaporation (Figure 15).

The simulations with `BlackHawk` allowed us to have a better understanding of the greybody factor $\Gamma_s(x)$. This function suppresses the particle emission with wavelengths much larger than the BH radius, i.e, the typical emitted particles of a Planckian thermal spectrum. As a consequence, the Hawking spectrum shifts the emission to higher energies as Figures 16 to 18 show. Indeed, most emitted photons from a BH have energies in the range $\overline{E} \sim 6\, kT$ (see Figure 19), while the most typical photons of a black body spectrum with temperature T_{BH} have energies $\overline{E} \sim kT$. In order to compare our total photon spectrum estimation, we used simulations with `BlackHawk` for the primary and secondary spectra, for PBHs with several lifetimes $\tau \leq 5$ years (see Table 1). We found that our estimations for the spectral emission rate and the time-integrated spectrum for photons are about the same size as those obtained with `BlackHawk`. Moreover, the simulations showed that our correction for the primary photon spectrum is correct, i.e, the spectral emission of primary photons has no dependence on the initial BH temperature when $E_\gamma \gtrsim 10\, kT_\tau$ (see Figure 24).

In order to identify a photon signature from a PBH evaporation, we obtained the number of photons that arrive at the Earth's atmosphere within certain energy intervals, that covered low and very high energies, for fixed observation time intervals. We noticed that a possible PBH signature is a VHE gamma ray burst of short duration, while gamma ray bursts (GRB) have durations that can be extended to hours. Another feature, is that VHE gamma rays from PBH evaporation can be detected locally, while GRBs and supernova explosions can be detected at cosmological distances (see Figure 25). Assuming that one of these photons could eventually reach the Earth, we did a basic study of the electromagnetic shower produced by these γ-rays using simulations in `Corsika`. As a future work, we plan to study the diffuse γ-ray signal due to other γ-ray sources to find a more accurate PBH photon signature. Also, we expect to study more deeply the extensive air showers using `Corsika` simulations, and including new techniques for reconstruction events such as machine learning.

Detecting photons from a PBH evaporation is a serendipitous task. However, a new generation of γ-ray observatories are under design and construction phase (CTA, SWGO). These instruments will bring us the opportunity to try new methods of detection, and to have better energy sensitivity (CTA) and better field of view (SWGO). Therefore, we are in time to prepare better strategies to detect PBH evaporation, or set new searching constraints. Hawking radiation is a remarkable feature that connects gravitation, thermodynamics, and quantum mechanics. However, there is still no experimental evidence, so it needs to be proved or discarded.

8 Acknowledgments

I would like to thank Prof. Claudio Dib for the guidance and the support. The countless physics discussions helped me to grow as a physicist and scientist. To my parents and brother, for their unconditional support and confidence. To my partner for sharing her life next to mine in this moment, and to my friends because you are part of this too. Finally, I would like to thank the physics department, and the graduate school of Universidad Técnica Federico Santa María, for the educational and financial support during these years.

9 Appendix: Calculation of quark hadronization into pions

To estimate the quark hadronization into pions, we need to obtain the total distribution of (u, d) quarks after the flavor quark changing through the $W^{\pm}$ decay (see Figure 32). The number per unit of time (hereafter the number) of q quarks in the energy interval $[E_q, E_q + dE_q]$ is

$$d\dot{N}_q = C^{(h)} \frac{(E_q/kT)^2}{e^{E_q/kT} + 1} dE_q \equiv f\left(\frac{E_q}{kT}\right) dE_q. \tag{138}$$

Following the decay process shown in Figure 32, the number of quarks per each flavor can be written as

$$\begin{aligned}
d\dot{N}_t &= d\dot{N}_t^{(BH)} \\
d\dot{N}_b &= d\dot{N}_b^{(BH)} + d\dot{N}_{b/t} \\
d\dot{N}_c &= d\dot{N}_c^{(BH)} + d\dot{N}_{c/b} \\
d\dot{N}_s &= d\dot{N}_s^{(BH)} + d\dot{N}_{s/c} \\
d\dot{N}_u &= d\dot{N}_u^{(BH)} + d\dot{N}_{u/s} + d\dot{N}_{u/c} + d\dot{N}_{u/b} \\
d\dot{N}_d &= d\dot{N}_d^{(BH)} + d\dot{N}_{d/s} + d\dot{N}_{d/c} + d\dot{N}_{d/b},
\end{aligned} \tag{139}$$

where $dN_q^{(BH)}$ is the primary emission, i.e, the quarks that are directly emitted by the BH, while $dN_{q/q'}$ is the number of q quarks produced by q' quark decay.

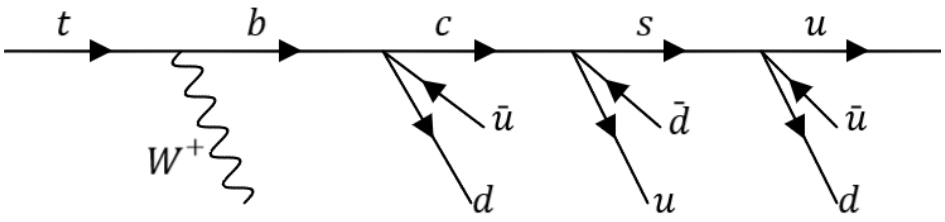

Figure 32: Approximate model of secondary (u, d) quark production given the flavor quark changing through the $W^{\pm}$ decay.

For convenience we shall define the following notation:

$$f_m \equiv m\, f\left(\frac{mE_q}{kT}\right), \tag{140}$$

that can be used only if the function $f(E_q/kT)$ is multiplied by the energy differential of the energy that appears in the f argument, i.e, dE_q. Thus, Equation (138) can be written now as

$$d\dot{N}_q = f_1\, dE_q. \tag{141}$$

Notice that under the change of variable $E_{q'} = E_q/n$

$$\begin{aligned} f_m\, dE_q &= m\, f\left(\frac{mE_q}{kT}\right) dE_q \\ &= (m \times n)\, f\left((m \times n)\,\frac{E_{q'}}{kT}\right) dE_{q'} \\ \therefore f_m\, dE_q &= f_{m\times n}\, dE_{q'} \quad , \quad E_{q'} = \frac{E_q}{n}. \end{aligned} \tag{142}$$

Let us calculate the number of each flavor quark of Equation (139):

- **top quark:** There is primary emission only. Thus

$$\begin{aligned} d\dot{N}_t &= d\dot{N}_t^{(BH)} \\ &= f\left(\frac{E_t}{kT}\right) dE_t \\ &= f_1\, dE_t. \end{aligned} \tag{143}$$

- **bottom quark:** There is primary and secondary emission

$$d\dot{N}_b = d\dot{N}_b^{(BH)} + d\dot{N}_{b/t}. \tag{144}$$

The number of primary b quarks in the energy interval $[E_b, E_b + dE_b]$ is:

$$\begin{aligned} d\dot{N}_b^{(BH)} &= f\left(\frac{E_b}{kT}\right) dE_b \\ &= f_1\, dE_b. \end{aligned} \tag{145}$$

The number of secondary b quarks (produced by t quark decay) in the energy interval $[E_b, E_b + dE_b]$ is related to the number of t quarks in the energy interval $[E_t, E_t + dE_t]$ through (see Figure 32)

$$\begin{aligned} d\dot{N}_{b/t}(E_b) &= 1\, d\dot{N}_t(E_t) \quad , \quad E_b = \frac{E_t}{2} \\ &= f\left(\frac{E_t}{kT}\right) dE_t \\ &= f_1\, dE_t \\ &= f_2\, dE_b, \end{aligned} \tag{146}$$

where in the last line we have used the property of Equation (142) given the change of variable $E_b = E_t/2$, such that $f_1\, dE_t = f_{2\times 1}\, dE_b$. Inserting Equations (145) and (146) in Equation (144), the total number of b quarks is:

$$d\dot{N}_b = (f_1 + f_2)\, dE_b. \tag{147}$$

- **charm quark:** Proceeding in analogous way, for c quark we obtain

$$\begin{aligned} d\dot{N}_c &= d\dot{N}_c^{(BH)} + d\dot{N}_{c/b} \quad , \quad E_c = \frac{E_b}{3} \\ &= d\dot{N}_c^{(BH)} + 1\, d\dot{N}_b \\ &= f_1\, dE_c + (f_1 + f_2)\, dE_b \\ &= (f_1 + f_3 + f_6)\, dE_c. \end{aligned} \tag{148}$$

- **strange quark:**

$$\begin{aligned} d\dot{N}_s &= d\dot{N}_s^{(BH)} + d\dot{N}_{s/c} \quad , \quad E_s = \frac{E_c}{3} \\ &= d\dot{N}_s^{(BH)} + 1\, d\dot{N}_c \\ &= f_1\, dE_s + (f_1 + f_3 + f_6)\, dE_c \\ &= (f_1 + f_3 + f_9 + f_{18})\, dE_s. \end{aligned} \tag{149}$$

- **up quark:**

$$\begin{aligned} d\dot{N}_u &= d\dot{N}_u^{(BH)} + d\dot{N}_{u/s} + d\dot{N}_{u/c} + d\dot{N}_{u/b} \quad , \quad E_u = \frac{E_q}{3} \ , \ q = s, c, b \\ &= d\dot{N}_u^{(BH)} + 2\, d\dot{N}_s + 1\, d\dot{N}_c + 1\, d\dot{N}_b \\ &= f_1\, dE_u + 2\,(f_1 + f_3 + f_9 + f_{18})\, dE_s + (f_1 + f_3 + f_6)\, dE_c + (f_1 + f_2)\, dE_b \\ &= (f_1 + 4f_3 + f_6 + 3f_9 + f_{18} + 2f_{27} + 2f_{54})\, dE_u. \end{aligned} \tag{150}$$

- **down quark:**

$$\begin{aligned} d\dot{N}_d &= d\dot{N}_d^{(BH)} + d\dot{N}_{d/s} + d\dot{N}_{d/c} + d\dot{N}_{d/b} \quad , \quad E_d = \frac{E_q}{3} \ , \ q = s, c, b \\ &= d\dot{N}_d^{(BH)} + 1\, d\dot{N}_s + 1\, d\dot{N}_c + 1\, d\dot{N}_b \\ &= f_1\, dE_d + (f_1 + f_3 + f_9 + f_{18})\, dE_s + (f_1 + f_3 + f_6)\, dE_c + (f_1 + f_2)\, dE_b \\ &= (f_1 + 3f_3 + f_6 + 2f_9 + f_{18} + f_{27} + f_{54})\, dE_d. \end{aligned} \tag{151}$$

From Equations (150) and (151) we can write the spectral emission rate of total u and d quarks. Using Equations (138) and (140) we obtain

$$\begin{aligned} \frac{d\dot{N}_u}{dE_u} = C^{(h)} \Bigg[& f\left(\frac{E_u}{kT}\right) + 12f\left(\frac{3E_u}{kT}\right) + 6f\left(\frac{6E_u}{kT}\right) + 27f\left(\frac{9E_u}{kT}\right) \\ & + 18f\left(\frac{18E_u}{kT}\right) + 54f\left(\frac{27E_u}{kT}\right) + 108f\left(\frac{54E_u}{kT}\right) \Bigg], \end{aligned} \tag{152}$$

$$\begin{aligned} \frac{d\dot{N}_d}{dE_d} = C^{(h)} \Bigg[& f\left(\frac{E_d}{kT}\right) + 9f\left(\frac{3E_d}{kT}\right) + 6f\left(\frac{6E_d}{kT}\right) + 18f\left(\frac{9E_d}{kT}\right) \\ & + 18f\left(\frac{18E_d}{kT}\right) + 27f\left(\frac{27E_d}{kT}\right) + 54f\left(\frac{54E_d}{kT}\right) \Bigg]. \end{aligned} \tag{153}$$

The total (u, d) quarks will hadronize into pions according to

$$\frac{d\dot{N}_\pi}{dE_\pi} = \sum_{q=u,d} \int_0^\infty dE \int_0^1 dz \, \frac{d\dot{N}_q}{dE} \, D_{\pi/q}(z) \, \delta(E_h - zE). \tag{154}$$

This integral can be solved taking advantage that

$$\frac{d\dot{N}_q}{dE_q} \propto m f\left(\frac{mE_q}{kT}\right). \tag{155}$$

Then

$$\begin{aligned} \frac{d\dot{N}_\pi}{dE_\pi} &\propto \sum_{q=u,d} \int_0^\infty dE_q \, m f\left(\frac{mE_q}{kT}\right) \int_0^1 dz \, D_{\pi/q}(z) \, \delta(E_\pi - zE_q) \\ &\propto \sum_{q=u,d} m \int_0^\infty \frac{d(mE_q)}{mE_q} \, f\left(\frac{mE_q}{kT}\right) \, D_{\pi/q}\left(\frac{mE_\pi}{mE_q}\right). \end{aligned} \tag{156}$$

Inserting the change of variable $x = mE_q/kT$, and the expression for the fragmentation function $D_{\pi/q}(z)$ defined in Equation (84)

$$\begin{aligned} \frac{d\dot{N}_\pi}{dE_\pi} &\propto \sum_{q=u,d} m \int_0^\infty dx \, \frac{f(x)}{x} \, D_{\pi/q}\left(\frac{mE_\pi}{kT}\frac{1}{x}\right) \\ &\propto \frac{15}{16} \int_0^\infty dx \, \frac{x}{e^x + 1} \left[m\left(\frac{mE_\pi}{kT}\frac{1}{x}\right)^{-3/2} - 2m\left(\frac{mE_\pi}{kT}\frac{1}{x}\right)^{-1/2} + m\left(\frac{mE_\pi}{kT}\frac{1}{x}\right)^{1/2} \right] \\ &\propto \frac{15}{16} \left[I(7) m\left(\frac{mE_\pi}{kT}\right)^{-3/2} - 2I(5) m\left(\frac{mE_\pi}{kT}\right)^{-1/2} + I(3) m\left(\frac{mE_\pi}{kT}\right)^{1/2} \right], \end{aligned} \tag{157}$$

where we have used the identity

$$I(s) = \int_0^\infty dx \, \frac{x^{s/2-1}}{e^x + 1} = \Gamma(s/2)\eta(s/2) = \Gamma(s/2)(1 - 2^{1-s/2})\zeta(s/2). \tag{158}$$

Inserting all terms of Equations (152) and (153) we finally obtain

$$\frac{d\dot{N}_{\pi}}{dE_{\pi}} = \frac{1215}{512\pi^3\hbar}\left[I(7)\,F_{-3/2}\left(\frac{E_{\pi}}{kT}\right) - 2I(5)\,F_{-1/2}\left(\frac{E_{\pi}}{kT}\right) + I(3)\,F_{1/2}\left(\frac{E_{\pi}}{kT}\right)\right] \tag{159}$$

where we have defined the function

$$\begin{aligned} F_m\left(\frac{E}{kT}\right) = 2\left(\frac{E}{kT}\right)^m + 21\left(\frac{3E}{kT}\right)^m + 12\left(\frac{6E}{kT}\right)^m + 45\left(\frac{9E}{kT}\right)^m \\ + 36\left(\frac{18E}{kT}\right)^m + 81\left(\frac{27E}{kT}\right)^m + 162\left(\frac{54E}{kT}\right)^m. \end{aligned} \tag{160}$$

Therefore, the approximate π^0 spectral emission rate given quark hadronization is:

$$\frac{d\dot{N}_{\pi^0}}{dE_{\pi^0}} = \frac{1}{3}\frac{d\dot{N}_{\pi}}{dE_{\pi}}. \tag{161}$$

10 References

[1] Alessandro De Angelis and Mário Pimenta. *Introduction to particle and Astroparticle Physics, Multimessenger Astronomy and its Particle Physics Foundations; 2nd edition*. Springer International Publishing, 2018.

[2] Alexandre Arbey and Jérémy Auffinger. "BlackHawk: a public code for calculating the Hawking evaporation spectra of any black hole distribution". *The European Physical Journal C*, 79(8):693, August 2019.

[3] Alexandre Arbey and Jérémy Auffinger. "Physics beyond the standard model with BlackHawk v2.0". *The European Physical Journal C*, 81(10):910, October 2021.

[4] Jacob D. Bekenstein. https://link.aps.org/doi/10.1103/PhysRevD.7.2333. *Phys. Rev. D*, 7:2333–2346, Apr 1973.

[5] Johannes Bellm, Stefan Gieseke, David Grellscheid, Simon Plätzer, Michael Rauch, Christian Reuschle, Peter Richardson, Peter Schichtel, Michael H Seymour, Andrzej Siódmok, Alexandra Wilcock, Nadine Fischer, Marco A Harrendorf, Graeme Nail, Andreas Papaefstathiou, and Daniel Rauch. Herwig 7.0/Herwig++ 3.0 release note. *The European Physical Journal C*, 76(4):196, April 2016.

[6] B. J. Carr. The primordial black hole mass spectrum. *Astrophysical Journal*, 201:1–19, October 1975.

[7] Bernard Carr and Florian Kuhnel. Primordial black holes as dark matter candidates. *SciPost Phys. Lect. Notes*, page 48, 2022.

[8] National Geophysical Data Center. NCEI geomagnetic calculators.

[9] Ivan Gonzalez, Igor Kondrashuk, Victor H. Moll, and Alfredo Vega. Analytic Expressions for Debye Functions and the Heat Capacity of a Solid. *Mathematics*, 10(10), 2022.

[10] Ivan Gonzalez and Victor H. Moll. Definite integrals by the method of brackets. Part 1. *Advances in Applied Mathematics*, 45(1):50–73, 2010.

[11] F. Halzen, E. Zas, J. H. MacGibbon, and T. C. Weekes. Gamma rays and energetic particles from primordial black holes. *Nature*, 353(6347):807–815, Oct 1991.

[12] S. W. Hawking. Black hole explosions? *Nature*, 248(5443):30–31, Mar 1974.

[13] S. W. Hawking. Particle creation by black holes. *Communications in Mathematical Physics*, 43(3):199–220, Aug 1975.

[14] D. Heck, J. Knapp, J. N. Capdevielle, G. Schatz, and T. Thouw. CORSIKA: A Monte Carlo code to simulate extensive air showers. 2 1998.

[15] R. López-Coto, M. Doro, A. de Angelis, M. Mariotti, and J.P. Harding. Prospects for the observation of Primordial Black Hole evaporation with the Southern Wide field of view Gamma-ray Observatory. *Journal of Cosmology and Astroparticle Physics*, 2021(08):040, aug 2021.

[16] Don N. Page. Particle emission rates from a black hole: Massless particles from an uncharged, nonrotating hole. *Phys. Rev. D*, 13:198–206, Jan 1976.

[17] V. B. Petkov, E. V. Bugaev, P. A. Klimai, M. V. Andreev, V. I. Volchenko, G. V. Volchenko, A. N. Gaponenko, Zh. Sh. Guliev, I. M. Dzaparova, D. V. Smirnov, A. V. Sergeev, A. B. Chernyaev, and A. F. Yanin. Searching for very-high-energy gamma-ray bursts from evaporating primordial black holes. *Astronomy Letters*, 34(8):509–514, Aug 2008.

[18] Bernard F. Schutz. *A FIRST COURSE IN GENERAL RELATIVITY*. Cambridge Univ. Pr., Cambridge, UK, 1985.

[19] Torbjörn Sjöstrand, Stefan Ask, Jesper R. Christiansen, Richard Corke, Nishita Desai, Philip Ilten, Stephen Mrenna, Stefan Prestel, Christine O. Rasmussen, and Peter Z. Skands. An introduction to PYTHIA 8.2. *Computer Physics Communications*, 191:159–177, 2015.

[20] Joaquín Miguel Sureda Hernández. Primordial black holes as dark matter, Oct 2021.

[21] T.N. Ukwatta, D.R. Stump, J.T. Linnemann, J.H. MacGibbon, S.S. Marinelli, T. Yapici, and K. Tollefson. Primordial Black Holes: Observational characteristics of the final evaporation. *Astroparticle Physics*, 80:90–114, 2016.

[22] R. L. Workman and Others. Review of Particle Physics. *PTEP*, 2022:083C01, 2022.

[23] Ya. B. Zel'dovich and I. D. Novikov. The Hypothesis of Cores Retarded during Expansion and the Hot Cosmological Model. *Astronomicheskii Zhurnal*, 43:758, January 1966.